CHARACTERIZING THE BIOMECHANICAL RESPONSE OF THE LIVER

ANTHONY CHARLES SANTAGO II

Thesis submitted to the Faculty of the
Virginia Polytechnic Institute and State University
in partial fulfillment of the requirements for the degree of

Master of Science
in
Biomedical Engineering

Stefan M. Duma, Ph.D., Chair
Joel D. Stitzel, Ph.D.
Warren N. Hardy, Ph.D.
Jessica L. Sparks, Ph.D.

April 27, 2010

Blacksburg, Virginia

Keywords: Bovine, Human, Liver, Injury, Freezing, Temperature, Tension, Compression

CHARACTERIZING THE BIOMECHANICAL RESPONSE OF THE LIVER

Anthony Charles Santago II

ABSTRACT

Motor vehicle collisions can result in life threatening liver injuries. Dummies are utilized to study injury in motor vehicle collisions; however, no crash test dummies are currently equipped to represent individual solid organs. This has increased the use of finite element models to help reduce these injuries; however, accurate material models need to be established to have accurate injury assessment using these models. This thesis presents a total of 4 studies that explore the biomechanical response of liver. The research on bovine liver is geared to understanding whether or not liver tissue can be frozen prior to testing and what environmental temperature the liver should be tested at. The first study utilized two bovine livers that were each divided in half and one half was tested at 75°F while the other half was tested at 98°F. A total of 24 tensile failure tests were performed on the parenchyma. It was determined that there were no statically significant differences between failure stresses and strains between the testing temperatures. To test the effects of freezing, tensile tests were performed on the parenchyma of a single bovine liver that was divided in half. One half was frozen and then thawed prior to tensile testing while the other was tested fresh. It was determined that freezing reduces average failure strain by 50%. The research on human liver was geared toward understanding the rate dependence during uniaxial tension tests and unconfined compression tests. Samples were constructed of only the parenchyma. A total of 7 livers were used to create the 51 tensile specimens and a total of 6 livers were used to obtain the 36 unconfined compression specimens. For the uniaxial tensile tests, average failure stresses ranged from 40.21 to 61.02 kPa while average failure strain ranged from 24% to 34%. For the unconfined compression tests, average failure stresses ranged from -165 to -203 kPa while average failure strain ranged from -46% to -61%. It is expected that the results presented in this thesis will: 1) Help establish correct transportation and procurement methodology for soft tissue mechanical testing. 2) Provide tension and compression material response of the human liver at multiple strain rates for use as material properties and injury tolerance values to validate finite element models.

TABLE OF CONTENTS

ABSTRACT ii
TABLE OF CONTENTS iii
LIST OF FIGURES v
LIST OF TABLES vii
CHAPTER 1 FREEZING AFFECTS THE MECHANICAL PROPERTIES OF BOVINE LIVER 1
ABSTRACT 1
INTRODUCTION 1
METHODS 2
RESULTS 5
DISCUSSION 7
CONCLUSIONS 8
ACKNOWLEDGEMENTS 9
REFERENCES 9
CHAPTER 2 THE EFFECT OF TEMPERATURE ON THE MECHANICAL PROPERTIES OF BOVINE LIVER 10
ABSTRACT 10
INTRODUCTION 10
METHODS 11
RESULTS 14
DISCUSSION 16
CONCLUSION 17
AWKNOLEDGEMENTS 17
REFERENCES 18
CHAPTER 3 EFFECT OF STRAIN RATE ON THE BIOMECHANICAL RESPONSE OF HUMAN LIVER PARENCHYMA TESTED IN UNIAXIAL TESNION 19
ABSTRACT 19
INTRODUCTION 19
METHODS 22
RESULTS 31
DISCUSSION 35
CONCLUSION 41
ACKNOWLEDGEMENTS 42
REFERENCES 42
CHAPTER 4 EFFECT OF STRAIN RATE ON THE BIOMECHANICAL RESPONSE OF HUMAN LIVER TESTED IN UNCONFINED COMPRESSION 45
ABSTRACT 45
INTRODUCTION 45
METHODS 48
RESULTS 54
DISCUSSION 57

CONCLUSIONS 61
ACKNOWLEDGEMENTS 62
REFERENCES 62

LIST OF FIGURES

Figure 1: Custom Made Slicing Jig and Blade Assembly. 3
Figure 2: Stamping Methodology. 4
Figure 3: Specimen Mounting Methodology. 4
Figure 4: Stress vs. Strain Plots for Fresh and Frozen Tests. 6
Figure 5: Characteristic Average for Fresh and Frozen Tests. 6
Figure 6: Custom Made Slicing Jig and Blade Assembly. 12
Figure 7: Stamping Methodology. 12
Figure 8: Specimen Mounting Methodology. 13
Figure 9: Stress vs. Strain for Liver 1: 98°F and 75°F 14
Figure 10: Stress vs. Strain for Liver 2: 98°F and 75° 14
Figure 11: Characteristic Averages for Liver 1: 98°F and 75°F 15
Figure 12: Characteristic Averages for Liver 2: 98°F and 75°F 15
Figure 13: Custom made slicing jig (left) and blade assembly (right) 23
Figure 14: Tissue Slicing Methodology 24
Figure 15: Dimensions of the specimen stamp 24
Figure 16: Stamp with associated stamping base 24
Figure 17: Specimen Stamping Methodology 25
Figure 18: The hot plate warms the tissue to approximately 37°C 26
Figure 19: The thermostat controls the two heaters which heat the chamber while the hot plate warms the tissue 26
Figure 20: Experimental Setup 27
Figure 21: Specimen Mounting Methodology 28
Figure 22: Location of Cameras and Typical Pre Test Posterior and Lateral Images 29
Figure 23: High-Speed Video Stills of a Typical Uniaxial Tension Test 32
Figure 24: Stress vs. Strain data for the tests conducted at 0.008 s^{-1} and associated characteristic average 33
Figure 25: Stress vs. Strain data for tests conducted at 0.089 s^{-1} and associated characteristic average 33
Figure 26: Stress vs. Strain data for tests conducted at 0.871 s^{-1} and associated characteristic average 34
Figure 27: Stress vs. Strain data for tests conducted at 9.524 s^{-1} and associated characteristic average 34
Figure 28: Characteristic Averages for Each Rate 35
Figure 29: Failure Stress Comparison between Uehara (1995) and Current Study 37
Figure 30: Failure Strain Comparison between Uehara (1995) and Current Study 37
Figure 31: Comparison of Failure Stress between Bovine Data and Current Study at Rate 3 38
Figure 32: Comparison of Failure Strain between Bovine Data and Current Study at Rate 3 39
Figure 33: Comparison of Failure Load per Unit Width between Brunon (2010) and Current Study 40
Figure 34: Comparison of Failure Strain between Brunon (2010) and Current Study 40
Figure 35: Custom Slicing Jig (left) and Blade Assembly (right) 49
Figure 36: Slice Creation Methodology 49
Figure 37: Specimen Creation Methodology 49
Figure 38: Testing Apparatus for Uniaxial Compression Tests 50
Figure 39: Typical Force versus Time Curve Showing Failure Location and Area of Load Redistribution 52

Figure 40: Stress vs. Strain data for the tests conducted at 0.008 s-1 and associated characteristic average 55
Figure 41: Stress vs. Strain data for the tests conducted at 0.074 s-1 and associated characteristic average 55
Figure 42: Stress vs. Strain data for the tests conducted at 0.776 s-1 and associated characteristic average 56
Figure 43: Stress vs. Strain data for the tests conducted at 8.011 s-1 and associated characteristic average 56
Figure 44: Characteristic Averages for Each Rate 57
Figure 45: Failure Stress Comparison between Tamura (2002) and Current Study 59
Figure 46: Failure Strain Comparison between Tamura (2002) and Current Study 60
Figure 47: Still Frames of a Typical Unconfined Compression Tests 61

LIST OF TABLES

Table 1: Fresh Tests 7
Table 2: Frozen Tests 7
Table 3: Specimen data for Liver 1: 98°F 15
Table 4: Specimen data for Liver 1: 75°F 15
Table 5: Specimen data for Liver 2: 98°F 16
Table 6: Specimen data for Liver 2: 75°F 16
Table 7: Two-sample T-Tests p values for strain and stress 16
Table 8: Subject Information 23
Table 9: Data Acquisition and High-Speed Video Sampling Rates by Loading Rate 28
Table 10: Two-tailed Student-t-test p-values for comparisons made in between each loading rate. 35
Table 11: Comparison of Tension Test Performed on Human Liver Parenchyma to Tension Tests Performed on Human Liver Capsule 41
Table 12: Subject Information 48
Table 13: Data Acquisition and Sampling Rates by Loading Rate 51
Table 14: Two-tailed Student-t-test p-values for comparisons made in between each loading rate. 57

CHAPTER 1
FREEZING AFFECTS THE MECHANICAL PROPERTIES OF BOVINE LIVER

ABSTRACT

The need to quantify the mechanical properties of human abdominal organs is becoming increasingly important in the automotive industry due to the large incidence of injuries to these organs as a result of motor vehicle crashes. The need to develop appropriate preservation and testing methodology is of particular importance because of how quickly abdominal organ tissues degrade after death. The purpose of this study was to determine the effects of freezing on the mechanical properties of bovine liver parenchyma in uniaxial tension. In the current study, one fresh, never frozen bovine liver was divided in half. One half was frozen and then thawed prior to preparation, and the other half tested immediately. Each half was sliced and stamped so that multiple parenchyma tension coupons were produced. A total of 16 failure tests were performed at an average strain rate of 0.07 s^{-1}, 8 fresh and 8 previously frozen, using a custom uniaxial tension system. The results showed that there was no statistically significant difference ($p=0.07$) in the average failure stress between fresh and previously frozen tissue. However, the average failure strain of the previously frozen tissue was found to be significantly less ($p<0.01$) than the average failure strain of the fresh tissue. It was concluded from these data that in order to obtain accurate tensile mechanical properties of bovine liver parenchyma, the liver must not be frozen prior to testing.

INTRODUCTION

The need to quantify and understand the mechanical properties of human abdominal organs is becoming increasingly important in the automotive industry because of the incidence of injuries to these organs in motor vehicle crashes. Several studies have been conducted to look at the incidence of injury to abdominal organs in automobile crashes (Augenstein et al. 2000; Bondy 1980; Elhagediab and Rouhana 1998). From these studies it can be concluded that approximately 5% of all injuries in automotive crashes are to the abdominal organs. Finite element models are becoming an integral part of studying these injuries, but for the models to be effective they must have biomechanically-based material properties. Since abdominal organ tissues degrade quickly

after death, it is imperative to evaluate tissue preservation techniques, specifically freezing, and develop appropriate testing methodologies in order to obtain accurate material property data.

A number of studies have investigated the effects of freezing on the response of soft tissue. Woo et al. (1986) conducted a series of tension failure tests on rabbit medial collateral ligaments (MCL) to determine the effects of freezing on the mechanical properties. The ligaments were preconditioned and then pulled to failure. The results showed no significant change in the cyclic stress behavior, failure strength, or failure strain between the fresh and frozen samples. Tamura et al. (2002) performed a series of preconditioning compression tests on porcine liver specimens to determine the effects of freezing on the mechanical response of the tissue. They found that the hysteresis loops obtained after freezing the samples, matched the hysteresis loops of the same samples before freezing. From these results, Tamura et al. (2002) concluded that freezing did not significantly change the mechanical properties of the tissue in compression. Van Ee et al. (1998) performed a series of room temperature versus previously frozen and thawed failure tension tests on the tibialis anterior muscle of New Zealand white rabbits. Their results showed that the difference in the failure stress was statistically significant between the tissue that had been frozen and the tissue that was never frozen.

Although there have been some studies that have investigated the effect of freezing on soft tissue, there have been no studies that have evaluated the effects of freezing on the mechanical properties of abdominal organ tissue in tension. The effects of freezing on soft tissue may vary due to differences in the cellular structure of the tissue, fluid content, and testing methodology. Therefore, the purpose this research was to determine the effects of freezing on the mechanical properties of bovine liver parenchyma tested in uniaxial tension.

METHODS

A total of 16 failure tension tests were performed on the parenchyma of one fresh, never frozen bovine liver. The liver was obtained from Animal Technologies (Tyler, Texas) and was received within 24 hours after death. After arrival, the liver was sectioned into the two equal halves. One half was prepared and tested immediately after arrival. The second half was frozen for 26 days

and then thawed prior to preparation. The frozen half was thawed by placing it in a saline bath at 75° F for 12 hours.

In order to obtain constant thickness slices of the liver parenchyma, a custom blade assembly and slicing jig were utilized (Figure 1). The spacing of the blades on the blade assembly and blade guides on the slicing jig were designed to obtain multiple slices of tissue with a constant thickness of 5 mm. First a square block of tissue was placed in the slicing jig. Then the blades on the blade assembly were aligned in the groves of the slicing jig. Slicing was performed in one smooth pass of the blades through the tissue block while minimizing downward force in order to avoid damaging or deforming the tissue. After slicing, the tissue was immersed in DMEM (Dulbecco's Modified Eagle's Medium) to maintain specimen hydration. It should be noted that in between each step of the sample preparation the tissue was immersed in the DMEM bath to maintain specimen hydration.

Figure 1: Custom Made Slicing Jig and Blade Assembly.

To ensure that the tissue samples would not fail next to the grips, a custom stamp and stamping base were designed in order to obtain "dog-bone" shaped specimens commonly used for uniaxial tension testing (Figure 2). A slice of tissue was placed on the stamping base and positioned with the use of a cut-out jig to obtain specimens devoid of any visible vasculature or defects. Once the tissue was positioned, the stamp was placed on top of the tissue using guide rods. A plastic block was then placed on top of the stamp and lightly struck several times so that the stamp would cut the tissue into the desired shape.

Figure 2: Stamping Methodology.

A detailed specimen mounting procedure was developed in order to minimize the confounding effects of shear due to improper specimen alignment and variations in initial specimen slack (Figure 3). First, the specimens were aligned with the main axis of the top grip and clamped while oriented horizontally. The top grip assembly was then mounted vertically in the test setup, allowing the specimen to hang under its own weight. Finally, the bottom of the tissue was aligned so that the axis of the specimen coincided with the main axis of the load cell and then clamped in place.

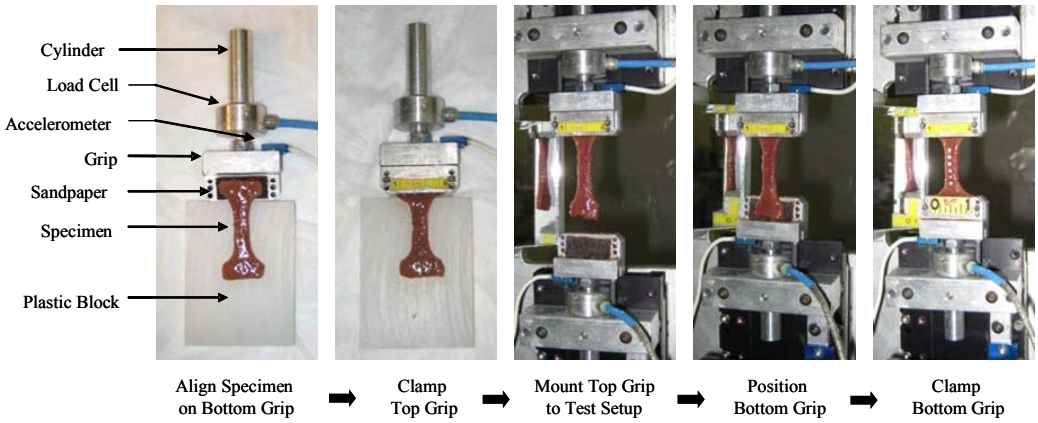

Figure 3: Specimen Mounting Methodology.

Once the coupons were mounted, posterior and lateral pretest pictures were taken with high resolution digital cameras, 470 pixels/in and 360 pixels/in respectively, in order to obtain initial width and thickness measurements. Equally spaced dots were then placed on the gage length in view of a high-speed camera, which was used to quantify strain and to confirm the location of the tear. During the test both the top and bottom grips simultaneously moved away from one another at a constant velocity to produce a strain rate of 0.07 s^{-1}. High-speed video of each test was recorded at 500 frames/sec with a resolution of 1600x1200 pixels, resulting in a pixel resolution of approximately 13 pixels/mm. All load cell and accelerometer data were sampled at 20 kHz.

The dots placed on the tissue were tracked throughout the duration of the test using motion analysis software (TEMA, Image Systems, Sweden). These data were then curve fit using a 5th degree polynomial and analyzed in an original Matlab code to determine the Green-Lagragian strain (ϵ) using the instantaneous distance between two dots (L_n), the original distance between the same two dots (L_o), and the stretch ratio (λ) (eq. 1, eq. 2). Strain was calculated for all dot combinations surrounding the failure tear. The dot combination closest to the failure tear was chosen to obtain a more localized failure strain. To calculate stress, the raw force data was first curve fit with a 5th degree polynomial. The 2nd Piola Kirchhoff Stress (S) was calculated using the instantaneous force (F) from the curve fit force, initial cross-sectional area at the location of the tear (A_o), and instantaneous stretch ratio (λ) (eq. 3). Finally, characteristic averages were then determined for both the fresh and frozen samples (Lessley et al. 2004).

$$\varepsilon = \frac{1}{2}\left(\lambda^2 - 1\right) \quad \textbf{eq. 1} \qquad \lambda = \frac{L_n}{L_o} \quad \textbf{eq. 2} \qquad S = \frac{F}{\lambda * A_o} \quad \textbf{eq. 3}$$

RESULTS

The 2nd Piola Kirchhoff Stress versus Green-Lagrangian strain curves for both the fresh and previously frozen specimens were plotted (Figure 4). Characteristic averages for both fresh and frozen coupons with associated standard deviations were plotted (Figure 5). Average dimensions and failure stress and strain values for each specimen were tabulated (Table 1, Table 2).

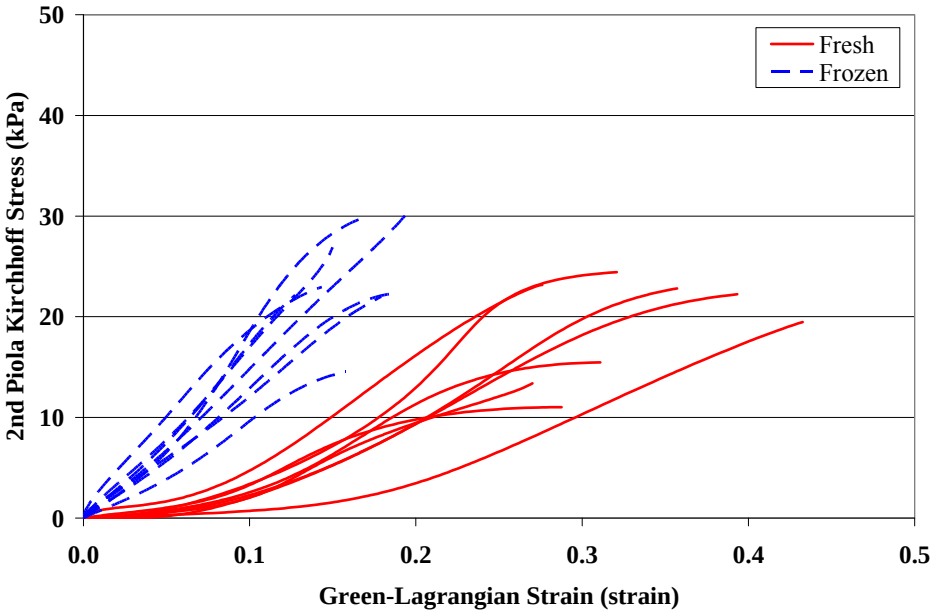

Figure 4: Stress vs. Strain Plots for Fresh and Frozen Tests.

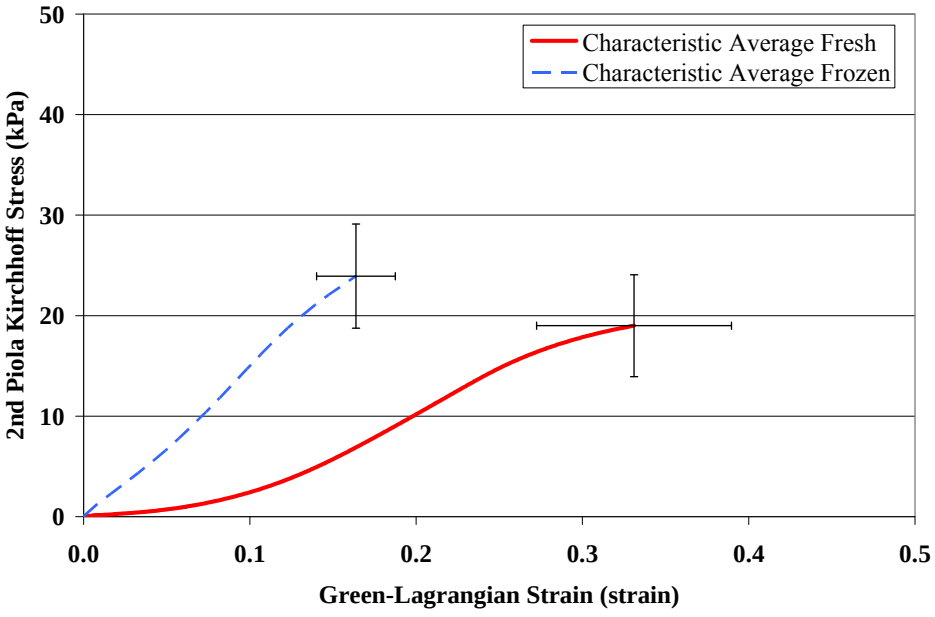

Figure 5: Characteristic Average for Fresh and Frozen Tests.

Table 1: Fresh Tests

Test	Width (mm)	Thickness (mm)	Area (mm^2)	Failure Strain (strain)	Failure Stress (kPa)
2	7.52	3.49	26.28	0.31	15.47
3	9.45	3.64	34.42	0.27	13.39
4	10.29	3.42	35.18	0.43	19.48
6	9.34	4.85	45.24	0.36	22.82
12	9.12	3.79	34.56	0.32	24.43
13	8.99	3.42	30.74	0.39	22.23
14	8.79	4.30	37.80	0.29	11.01
18	8.95	5.47	48.94	0.28	23.16
Avg	**9.06**	**4.05**	**36.64**	**0.33**	**19.00**
Std	**0.72**	**0.71**	**6.90**	**0.05**	**4.74**

Table 2: Frozen Tests

Test	Width (mm)	Thickness (mm)	Area (mm^2)	Failure Strain (strain)	Failure Stress (kPa)
2	8.48	3.73	31.62	0.14	22.94
3	8.89	3.73	33.15	0.20	30.78
4	10.94	3.67	40.17	0.17	29.76
5	7.77	3.73	28.95	0.19	22.38
14	8.07	3.62	29.21	0.15	26.91
15	10.32	4.49	46.40	0.18	22.25
16	8.59	3.78	32.47	0.16	14.55
17	9.71	3.73	36.19	0.13	22.15
Avg	**9.10**	**3.81**	**34.77**	**0.16**	**23.96**
Std	**1.05**	**0.26**	**5.58**	**0.02**	**4.84**

A paired, two-tailed Student's t-test was performed to determine if there were statistically significant differences in failure stress or strain between fresh and previously frozen samples. Significance was defined as a two-tailed p-value of ≤ 0.05. Fresh samples were found to have significantly ($p<0.01$) higher average failure strain than samples that were previously frozen. However, there was no statistical difference ($p=0.07$) in the average failure stress between the fresh and previously frozen samples.

DISCUSSION

In the this study, freezing effects on the tensile mechanical properties of bovine liver were evaluated by performing matched tests on fresh and previously frozen parenchyma samples obtained from the same liver. The samples from the frozen half of the liver were found to have a 49% lower failure strain ($p<0.01$) than the samples processed from the half which was never frozen. However, there was no statistically significant difference ($p=0.07$) in the failure stress between the fresh and previously frozen samples. The difference in the failure strain was most likely due to cellular damage as a result of water expansion during the freezing process. Future histology-based studies should be performed to analyze the extent of damage to the cellular structure of liver parenchyma as a result of freezing.

Although the results of the this study differ from previous studies that have shown no significant differences in the mechanical properties of fresh versus previously frozen soft tissue, the type of tissue and test methodology must be taken into account. Woo et al. (1986) demonstrated that there was no significant difference in the tensile material properties of fresh versus previously frozen rabbit medial collateral ligaments. Ligaments are constructed primarily of long pieces of type 1 collagen fibers and have low fluid content; therefore, the fibers would be only slightly damaged or not damaged at all during the freezing process due to the small amount of fluid that is retained in ligaments. Conversely, bovine liver parenchyma is constructed of hexagonal arranged hepatocyte cells with little connective tissue binding the cells together. In addition, the liver retains a significant amount of fluid which can expand during the freezing process, thereby damaging the cellular structure. Tamura et al (2002) demonstrated that there was no considerable difference in the compressive response of the fresh versus previously frozen samples of porcine liver parenchyma. Compressing soft tissue samples is different than pulling them apart; therefore, any cellular damage that might have been caused by the freezing process may have no effect on the compressive response of soft tissue. Tamura et al. (2002) based his conclusion on the hysteresis loops of matched specimens after 5 cycles of sub-failure preconditioning; therefore, it is possible that the preconditioning of the tissue may have caused structural changes in the tissue which could have effectively masked any changes in the compressive response that resulted from the freezing process. Van Ee et al. (1998) demonstrated a statistically significant difference between the failure tensile stress of rabbit anterior tibialis muscle that was frozen and then thawed versus rabbit anterior tibialis muscle that was never frozen. The failure properties of the rabbit muscle, however, were all determined after a significant amount of time in a room temperature environment (54-72 hours), which might have allowed for significant tissue degradation. Given that the structure of muscle tissue is considerably different from liver tissue, making a direct comparison be between the two studies is difficult.

CONCLUSIONS

A total of 16 tensile failure tests were conducted on the parenchyma of a bovine liver to test the effects of freezing on the tensile mechanical properties of bovine liver parenchyma. One bovine liver was sectioned into the two equal halves. One half was prepared and tested immediately

after arrival. The second half was frozen for 26 days before being thawed prior to preparation. Slices were cut from the parenchyma, stamped into the desired tension coupon shape, and pulled to failure. The 2nd Piola Kirchhoff Stress and Green-Lagrangian strain were calculated for each failure test. The average failure strain of the previously frozen tissue was found to be significantly less ($p<0.01$), approximately 49% less, than the average failure strain of the fresh tissue. Conversely, there was no statistical difference ($p=0.07$) found between the average failure stress of fresh versus previously frozen tissue. It was concluded from these data that in order to obtain accurate tensile mechanical properties of bovine liver parenchyma, the liver must not be frozen prior to testing.

ACKNOWLEDGEMENTS

The author would like to acknowledge the Toyota Motor Corporation for funding and support.

REFERENCES

CHAPTER 2
THE EFFECT OF TEMPERATURE ON THE MECHANICAL PROPERTIES OF BOVINE LIVER

ABSTRACT

Abdominal organ injuries account for approximately 3-5% of all injuries in automobile accidents. Because of this incidence of injury, understanding the mechanical properties of these organs is vital to preventing and treating these injuries. Abdominal organs degrade quickly after death and therefore the need to develop appropriate procurement and testing methodologies is imperative. The purpose of the work described here was to collect data from uniaxial tension tests to determine the effects of testing temperature on the mechanical properties of bovine liver parenchyma. Slices were taken from the parenchyma of two fresh, never frozen bovine livers and stamped into a tension coupon. The specimens for each liver were then divided into two groups. One group was tested in an environment held at 98°F and the other tested in an environment held at 75°F. A total of 13 failure tests were preformed at 98° F, physiological temperature, and a total of 11 failure tests were conducted at 75°F, which corresponds to room temperature. There was no statistical difference in the failure stress and strain ($p \geq 0.05$) for either of the two livers between the two temperatures. This shows that the calculated mechanical properties are not dependent on testing temperature in this range.

INTRODUCTION

Abdominal organ injuries account for approximately 3-5% of all injuries in automobile accidents (Augenstein et al. 2000; Bondy 1980; Elhagediab and Rouhana 1998). Because of this high incidence of injury, understanding the mechanical properties of these organs is vital to preventing and mitigating these injuries. Accurate material properties of the abdominal organs need to be obtained in order to develop acceptable finite element models of the human body. The need to determine if testing at body temperature makes a difference in the mechanical response is imperative to developing accurate material properties.

Although a number of studies have investigated the effect of temperature on the mechanical properties of soft tissue, results of these studies vary depending on the temperature range. Woo et

al. (1987) performed tensile tests on canine medial collateral ligaments under a range of temperatures, 2°C and 37°C and reported that the mechanical response of the ligament varied with respect to temperature. Similarly, Bass et al. (2007) reported that the tensile material properties of porcine lumbar spine ligaments varied between 5°C and 38°C. Dorlot et al. (1980) concluded that the mechanical properties of anterior cruciate canine ligaments did not show any difference in the range of 23°C to 45°C. Similarly, Hasberry and Pearcy (1986) concluded that the material response of interspinous ligaments of sheep did not vary in a temperature range of 19°C to 46°C (Hasberry and Pearcy 1986).

The varying results of the previous studies demonstrate a need to determine the effect of temperature in the range desired. In addition, the structural differences between ligaments and soft tissue might affect the results. Therefore, the purpose of this research was to collect data from uniaxial tension tests to determine the effects of testing temperature on the mechanical properties of bovine liver parenchyma between 98°F and 75°F.

METHODS

A total of 24 failure tension tests were preformed on the parenchyma of two fresh, never frozen bovine livers. Livers were obtained from Animal Technologies (Tyler, Texas) and were received within 24 hours after procurement. After arrival, the livers were sectioned into two equal halves. One half was tested at body temperature (98°F) while the other was tested at room temperature (75°F).

To obtain constant thickness slices of the liver parenchyma, a custom blade assembly and slicing jig were utilized (Figure 6). The spacing of the blades on the blade assembly and blade guides on the slicing jig were designed to obtain multiple slices of tissue with a constant thickness of 5 mm. First a square block of tissue was placed in the slicing jig. Then the blades on the blade assembly were aligned in the groves of the slicing jig. The slicing was performed in one smooth pass of the blades through the tissue block while minimizing downward force in order to avoid damaging or deforming the tissue. After slicing, the tissue was then immersed in DMEM (Dulbecco's Modified Eagle's Medium) to maintain specimen hydration. It should be noted that

in between each step of the sample preparation the tissue was immersed in the DMEM bath to maintain specimen hydration.

Figure 6: Custom Made Slicing Jig and Blade Assembly.

To ensure that the tissue samples would not fail next to the grips, a custom stamp and stamping base were designed in order to obtain "dog-bone" shaped specimens commonly used for uniaxial tension testing (Figure 7). A slice of tissue was placed on the stamping base and positioned with the use of a cut out jig in order to obtain specimens devoid of any vasculature or defects. Once the tissue was positioned, the stamp was placed on top of the tissue using guide rods. Finally, a plastic block was then placed on top of the stamp and lightly struck several times with a hammer so that the stamp would cut the tissue into the desired shape.

Figure 7: Stamping Methodology.

A detailed specimen mounting procedure was developed in order to minimize the confounding affects of shear, due to improper specimen alignment, and variations in initial specimen slack (Figure 8). First, the specimens were aligned with axis of the top grip and clamped while oriented horizontally. The top grip assembly was then mounted vertically in the test setup, allowing the specimen to hang under its own weight. Finally, the bottom of the tissue was aligned so that the axis of the specimen coincided with the main axis of the load cell and then clamped in place.

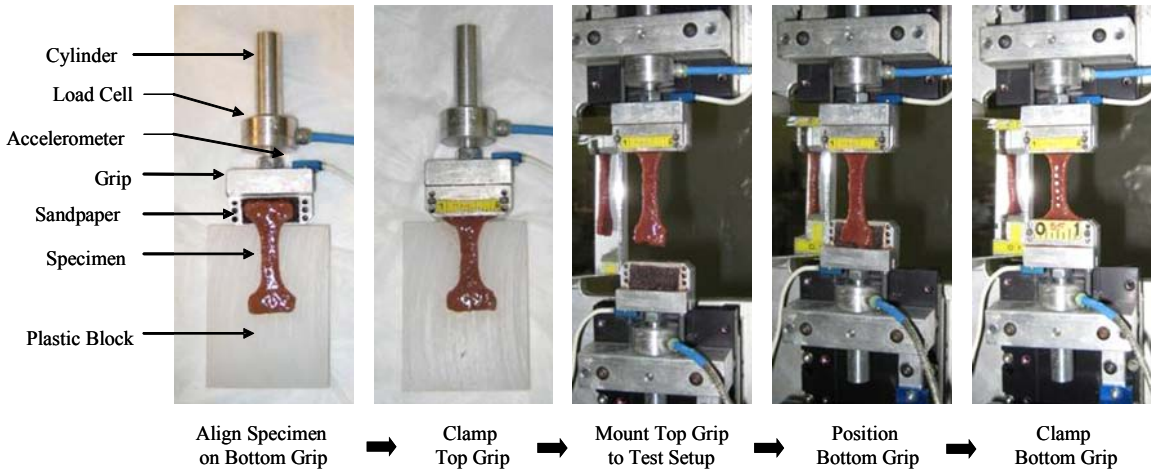

Figure 8: Specimen Mounting Methodology.

Once the coupons were mounted, posterior and lateral pretest pictures were taken with high resolution digital cameras, 470 pixels/in and 360 pixels/in respectively, in order to obtain initial width and thickness measurements. Equally spaced dots were then placed on the gage length in view of a high-speed camera, which was used to quantify strain and to confirm the location of the tear. During the test both the top and bottom grips simultaneously moved away from one another at a constant velocity to produce a strain rate of 0.07 s^{-1}. High-speed video of each test was recorded at 500 frames/sec with a resolution of 1600x1200 pixels, which resulted in a pixel resolution of approximately 13 pixels/mm. All load cell and accelerometer data was sampled at 20 kHz.

The dots placed on the tissue were tracked throughout the duration of the test using motion analysis software (TEMA, Image Systems, Sweden). These data were then curve fit using a 5^{th} degree polynomial and analyzed in an original Matlab code to determine the Green-Lagragian strain (ϵ) using the instantaneous distance between two dots (L_n), the original distance between the same two dots (L_o), and the stretch ratio (λ) (eq. 4, eq. 5). Strain was calculated for all dot combinations surrounding the failure tear. The dot combination closest to the failure tear was chosen to obtain a more localized failure strain. To calculate stress, the raw force data was first curve fit with a 5^{th} degree polynomial. The 2^{nd} Piola Kirchhoff Stress (S) was then calculated using the instantaneous force (F) from the curve fit force data, initial cross-sectional area at the location of the tear (A_o), and instantaneous stretch ratio (λ) (eq. 6). Finally, characteristic averages were then determined for both the fresh and frozen samples (Lessley et al. 2004).

$$\varepsilon = \frac{1}{2}\left(\lambda^2 - 1\right) \quad \textbf{eq. 4} \qquad \lambda = \frac{L_n}{L_o} \quad \textbf{eq. 5} \qquad S = \frac{F}{\lambda * A_o} \quad \textbf{eq. 6}$$

RESULTS

The 2nd Piola Kirchhoff Stress versus Green-Lagrangian strain was plotted for both the body temperature and room temperature tests for both subjects (Figure 9, Figure 10). The characteristic averages for both livers were also plotted (Figure 11, Figure 12). Width and thickness values were tabulated along with the failure stress and strain for each test (Table 3, Table 4, Table 5, Table 6). A series of two-tailed t tests, assuming unequal variance, were preformed to determine if there were any significant differences in failure stress and strain due to temperature for each respective liver (Table 7). An additional t-test was preformed to determine if there was any significant difference due to subject variation, i.e. Body 1 versus Body 2. Significance was defined as a two-tailed-p-value of $\leq$0.05.

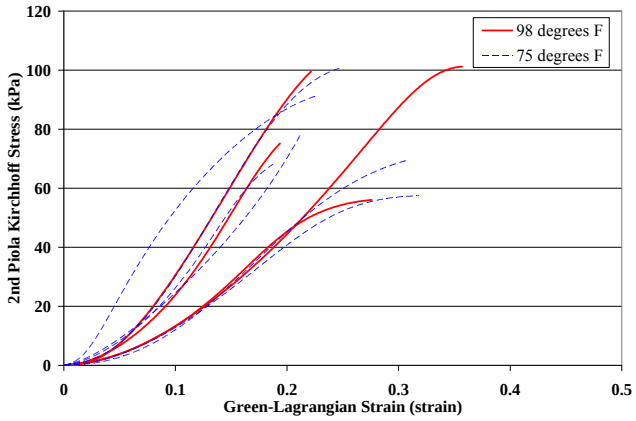

Figure 9: Stress vs. Strain for Liver 1: 98°F and 75°F

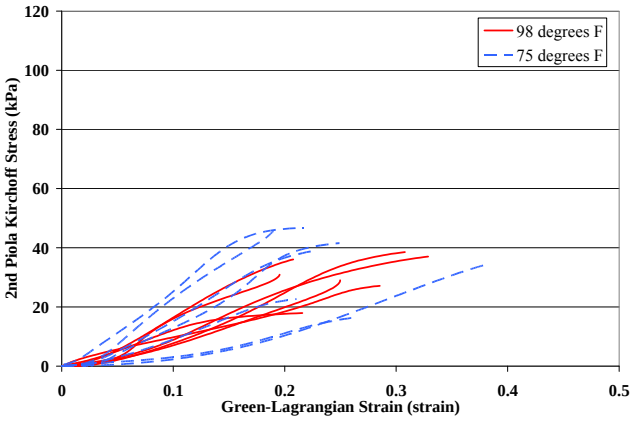

Figure 10: Stress vs. Strain for Liver 2: 98°F and 75°

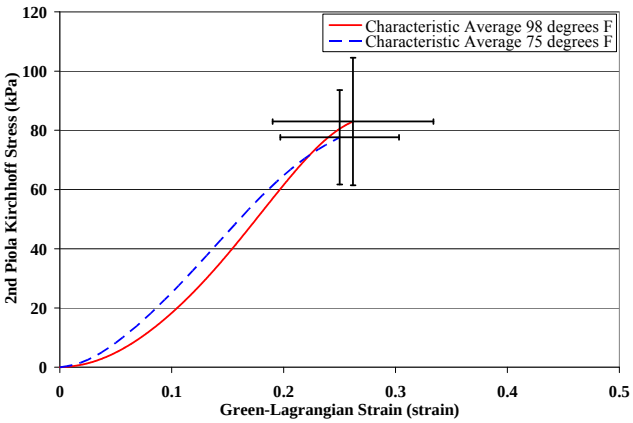

Figure 11: Characteristic Averages for Liver 1: 98°F and 75°F

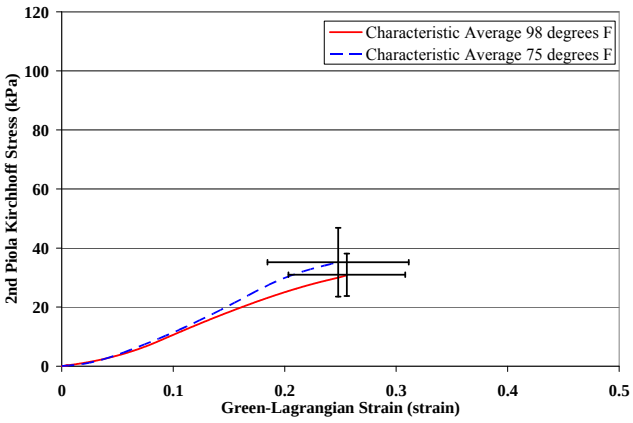

Figure 12: Characteristic Averages for Liver 2: 98°F and 75°F

Table 3: Specimen data for Liver 1: 98°F

Test	Width (mm)	Thickness (mm)	Area (mm^2)	Max Strain (strain)	Max Stress (kPa)
91	7.86	4.87	38.28	0.28	56.04
94	6.85	4.45	30.48	0.22	99.53
95	8.27	4.02	33.25	0.36	101.20
96	7.46	4.02	29.99	0.19	75.17
Avg	**7.61**	**4.34**	**33.00**	**0.26**	**82.98**
Std	**0.61**	**0.41**	**3.80**	**0.07**	**21.55**

Table 4: Specimen data for Liver 1: 75°F

Test	Width (mm)	Thickness (mm)	Area (mm^2)	Max Strain (strain)	Max Stress (kPa)
82	6.65	3.18	21.15	0.31	69.64
83	8.27	4.23	34.98	0.25	100.61
84	7.26	4.02	29.19	0.32	57.46
86	8.67	4.23	36.67	0.21	78.98
87	7.26	4.45	32.31	0.19	68.10
88	7.46	3.60	26.86	0.23	91.11
Avg	**7.60**	**3.95**	**30.19**	**0.25**	**77.65**
Std	**0.74**	**0.47**	**5.72**	**0.05**	**15.96**

Table 5: Specimen data for Liver 2: 98°F

Test	Width (mm)	Thickness (mm)	Area (mm^2)	Max Strain (strain)	Max Stress (kPa)
7	8.57	3.50	30.00	0.29	27.13
9	9.17	4.08	37.41	0.20	30.96
10	8.14	3.64	29.63	0.31	38.55
11	8.52	4.15	35.36	0.22	17.96
12	8.46	3.35	28.34	0.33	37.07
13	8.92	3.13	27.92	0.25	29.01
15	9.75	3.28	31.98	0.21	36.08
Avg	**8.79**	**3.59**	**31.52**	**0.26**	**30.97**
Std	**0.54**	**0.39**	**3.62**	**0.05**	**7.17**

Table 6: Specimen data for Liver 2: 75°F

Test	Width (mm)	Thickness (mm)	Area (mm^2)	Max Strain (strain)	Max Stress (kPa)
5	8.32	4.59	38.19	0.38	34.37
10	8.48	2.92	24.76	0.22	46.67
12	10.52	3.28	34.51	0.21	22.66
15	8.65	2.99	25.86	0.19	45.73
16	7.82	4.45	34.80	0.23	39.01
17	8.04	3.86	31.03	0.26	16.28
21	8.85	3.50	30.98	0.25	41.59
Avg	**8.67**	**3.66**	**31.45**	**0.25**	**35.19**
Std	**0.89**	**0.67**	**4.87**	**0.06**	**11.64**

Table 7: Two-sample T-Tests p values for strain and stress

Mean Comparison	P value Strain	P value Stress
Body 1 vs. Body 2: 98°F	0.871	0.001
Body 1 vs. Body 2: 75°F	0.947	0.001
Body 1: 9°F 8 vs. 75°F	0.770	0.663
Body 2: 98°F vs. 75°F	0.805	0.430

DISCUSSION

In the current study, the effects of testing temperature on the mechanical properties of bovine liver parenchyma as well the affect of subject variation were evaluated. The failure stress was found to be significantly different between Body 1 and Body 2 at both 98°F and 75°F. The results of the current study show that there was no statistical difference in either stress or strain between 98°F and 75°F test environments. It was determined from these data that testing bovine liver in a temperature range between 98°F and 75°F would not change the mechanical properties of the tissue. Although the average failure properties where not found to be statistically different with respect to temperature, the tests preformed at 75°F showed a larger standard deviation in the average stress values than that of the tests preformed at 98°F for both livers. This would suggest

that testing at body temperature would produce slightly less scatter than testing at room temperature.

Although the current study found similar results to Dorlot et al. (1980) and Hasberry et al. (1986), it differs from the conclusions obtained in the Woo et al. (1987) and Bass et al. (2007) studies. These differing results are most likely due to temperature ranges used in the five studies. The current study as well as the Dorlot et al. (1980) and Hasberry et al. (1986) studies did not include testing temperatures close to freezing as those conducted by Bass et al. (2007) and Woo et al. (1987). This study does not directly compare to any of these previous studies; however, because the cellular composition of ligaments is much different than that of the liver. Ligaments are constructed of long pieces of type 1 collagen fibers while the liver parenchyma is constructed of hexagonal arranged hepatocyte cells with little connective tissue.

CONCLUSION

Failure tests on 24 tension coupons from the parenchyma of two bovine livers were used to determine the effect of temperature on the mechanical response of bovine liver tissue. After arrival, the livers were sectioned into two equal halves. One half was tested at body temperature (98°F) while the other was tested at room temperature (75°F). Slices were taken from the parenchyma, stamped, into the desired tension coupon shape, and the pulled to failure. The 2nd Piola Kirchhoff Stress and Green-Lagrangian strain were calculated for all of the test specimens. Characteristic averages were then computed for each organ at each temperature. A statistically significant difference was not found for either failure stress or strain for either organ with respect to temperature. There was, however, slightly more scatter in the tests preformed 75°F than at 98°F. From these results it can be concluded that between 98°F and 75°F testing temperature has no effect on the mechanical properties of bovine liver tissue.

AWKNOLEDGEMENTS

The author would like to acknowledge the Toyota Motor Corporation for their funding and support.

REFERENCES

Augenstein JS, Bowen J, Perdeck EB, Singer M, Stratton JE, Horton T, Rao A, Digges KH, Malliaris AC, Steps J. 2000. Injury patterns in near-side collisions. SAE 2000 World Congress: SAE International.

Bass CR, Planchak CJ, Slazar RS, Lucus SR, Rafaels K, Shender BS, Paskoff G. 2007. The Temperature-Dependent Viscoelasticity of Porcine Lumbar Spine Ligaments. SPINE 32(16):E436-E442.

Bondy N. 1980. Abdominal Injuries in the National Crash Severity Study. National Center for Statistics and Analysis. 59-80 p.

Dorlot JM, Ait Ba Sidi M, Tremblay G, Drouin G. 1980. Load Elongation Behavior of the canine anterior curciate ligament. Journal of Biomedical Engineering 102:190-193.

Elhagediab AM, Rouhana SW. Patterns of Abdominal Injury in Frontal Automotive Crashes; 1998; Windsor, Ontario, Canada.

Hasberry S, Pearcy MJ. 1986. Temperature dependence of the tensile properties of interspinous ligaments of sheep. Journal of Biomedical Engineering 109:68-71.

Lessley D, Crandall J, Shaw G, Funk J, Kent R. 2004. A Normalization Technique for Developing Corridors from Individual Subject Responses. SAE Technial Paper Series. Detriot, MI.

Woo SL-Y, Lee T, Gomez M. 1987. Temperature dependent behavior of the canine medial collateral ligament. Journal of Biomechanical Engineering 8(1):62-66.

CHAPTER 3
EFFECT OF STRAIN RATE ON THE BIOMECHANICAL RESPONSE OF HUMAN LIVER PARENCHYMA TESTED IN UNIAXIAL TESNION

ABSTRACT

Motor vehicle collisions can result in life threatening liver injuries. Crash dummies are utilized to study injury in motor vehicle collisions; however, no crash test dummies are currently equipped to represent individual solid organs. This has increased the use of finite element models to help reduce these injuries; however, accurate material models need to be established to have accurate injury assessment using these models. This study presents a total of 51 uniaxial tensile tests on the parenchyma of human liver. A total of 7 livers were utilized to acquire dog-bone shaped specimens for testing at four distinct strain rates: 0.008 s^{-1}, 0.089 s^{-1}, 0.871 s^{-1}, and 9.524 s^{-1}. All tests were performed within 48 hours of death. Load and acceleration data were obtained at the grip locations. Optical markers were tracked with a high-speed camera and used to determine local deformation. 2nd Piola Kirchhoff Stress and Green-Lagrangian strain were tabulated for each test. Rate dependence was seen with failure stress increasing and failure strain decreasing with increasing strain rate. Average failure stress ranged from 40.21 to 61.02 kPa while average failure strain ranged from 24% to 34%. This study provides failure properties and material response information for the parenchyma of the human liver at static, quasistatic, and dynamic loading rates for use as material properties and injury tolerance values to create finite element models.

INTRODUCTION

Although injuries to the abdomen account for only 3-5% of all injuries in motor vehicle collisions (MVCs), abdominal injuries constitute 8% of AIS 3+, 16.5% of AIS 4+, and 20.5% of AIS 5+ injuries (Augenstein et al. 2000; Bondy 1980; Elhagediab and Rouhana 1998). The most frequently injured abdominal organ in MVCs is the liver, which accounts for approximately 38% of all abdominal injuries (Elhagediab and Rouhana 1998). The mortality rate for blunt liver injuries ranges from 9-17% but can be as high as 67% if the inferior vena cava or the hepatic veins are involved (Christmas et al. 2005; Hurtuk et al. 2006; John et al. 1992). Holbrook et al. (2007) utilized the Crash Injury Research and Engineering Network (CIREN) to analyze liver

injuries and determined that 47% of all liver injuries in MVCs are of either moderate or major severity. Holbrook et al. (2007) also reported that the majority of the liver injuries were lacerations (81%). Thor (2008), utilized that National Automotive Sampling System / Crashworthiness Data System (NASS/CDS) to analyze injuries in frontal crashes and determined that, with and without the presence of airbags, lacerations accounted for 96% of all injuries to the liver. Currently, no crash test dummies used to assess injury risk in MVCs are equipped to represent individual solid organs located asymmetrically in the human abdomen (Tamura et al. 2002). Because of this, finite element models (FEMs) are being utilized to help reduce automotive related abdominal injuries. However, for FEMs to provide an accurate representation of the human livers response to a blunt impact and correctly predict injury, they must be validated based on physical variables mechanically related to injury, such as stress and strain.

Multiple studies have been performed to address the mechanical response of whole livers to impact. Melvin et al. (1973) performed *in vivo* local impacts on livers of 17 Rhesus monkeys. The liver was excised from each monkey and placed on a load cell while still being perfused by the living animal. An electrohydraulic servo-controlled impactor was used to impact the livers. Ram displacement was varied to produce strains from 40-74%. Loading rate was varied from 5 cm/s to 500 cm/s. It was determined that the stress-strain behavior of the liver was affected by the loading rate and onset of moderate trauma to the liver occurred at a stress level of 310 kPa. It was reported that for high rate tests subcapsular hemorrhaging, tears, and fractures were seen. Wang et al. (1992) performed force-relaxation and creep experiments on diseased and nondiseased porcine livers using an indenter. It was demonstrated that porcine liver tissue was a typical viscoelastic material and that normal and non-normal liver tissue had different biomechanical properties. Kerdok (2006) tested 4 porcine livers using a creep indention test. Each liver was impacted in-vivo, ex-vivo perfused, and ex-vivo nonperfused. The elastic and viscous responses were shown to be affected by perfusion. The biomechanical properties of the ex vivo perfused liver were shown to be similar to that of the in vivo perfused liver. However, the non-perfused livers were stiffer and more viscous and showed permanent strain deformation with repeated impacts. Sparks et al. (2007) impacted 14 fresh human livers with a rigid metal plate to a maximum deflection of 30% from the livers highest point. Peak applied stress varied between 157 kPa and 690 kPa with an average of 427 kPa to produce a MAIS 3+ injury. Impact

energy and strain rate were highly correlated to injury; however, the product of peak rate of tissue pressure increase and peak tissue pressure was shown to be the strongest correlate to injury. Lacerations were seen on all but one liver and corresponded to injuries seen in CIREN cases. Impacts to intact livers have demonstrated the viscoelastic characteristics of liver tissue, have shown that perfusion levels affect the material properties of liver tissue, and have revealed that the best indicator of injury is internal pressure in the parenchyma. However, these tests are limited by their ability to accurately calculate localized stress and strain. Therefore, in order to account for proper stress-strain relationships needed for FEMs, tissue level tension and compression tests need to be performed.

A number of studies have been performed to investigate the tensile material properties of liver tissue. Yamada (1970) tested rabbit liver parenchyma in uniaxial tension and reported an ultimate tensile strength of rabbit liver parenchyma to be 2.4 g/mm^2 (23kPa) with the ultimate percent elongation determined to be 46%. A hardness number of 0.38 was also reported. However, strain rate was not reported. Uehara (1995) tested 384 samples of porcine liver parenchyma in uniaxial tension. Tests were performed at loading rates of 5mm/min, 20mm/min, 50 mm/min, 200 mm/min, and 500 mm/min. True tensile failure stress ranged from 126 kPa to 205 kPa and increased as strain rate increased. Young's Modulus ranged from 0.684 MPa to 1.19 MPa and increased as strain rate increased. Extension ratio ranged from 1.29 to 1.26 and was shown to decrease with increased strain rate. Stingl et al. (2002) tested tissue strips from 15 livers taken from non-embalmed cadavers, and the breaking stress varied from 88 kPa to 322 kPa and relative elongation varied from 9.9% to 25%. There were no statistically significant differences seen between the failure breaking properties of male and female livers. However, it was not stated if the samples included only parenchyma and strain rate was not reported. Hollenstein et al. (2006) performed uniaxial tension tests on the capsule of one bovine liver. Capsule was removed from the parenchyma prior to testing. They reported that nominal stress was 9.2 ± 0.7 MPa and nominal strain was 35.6 ± 5.2%. Santago et al. (2009a) performed tensile tests on the parenchyma of bovine livers to determine the effect of testing temperature. A strain rate of 0.7 s^{-1} was utilized for these tests. They determined that there was no statistically significant difference found between failure stress and strain between specimens tested at 75°F versus those tested at 98°F. Average failure stress and strain for all samples in the study was 52.5

kPa and 25% respectively. Santago et al. (2009b) also performed tensile tests on bovine liver parenchyma to evaluate the affects of freezing. A strain rate of 0.7 s^{-1} was also utilized. They reported that freezing the tissue prior to testing significantly decreases failure strain. Brunon et al. (2010) performed uniaxial tension tests on porcine and human liver tissue. Each sample consisted of parenchyma and capsule. A displacement velocity of 0.5 mm/sec was utilized, which gave strain rates ranging from of 0.001 s^{-1} to 0.01 s^{-1}. Each sample was covered with a random pattern of white dots of matt paint in order to calculate failure strain. An ultimate load per width unit was determined to be 0.22 ± 0.14 N/mm for human tissue and 0.40 ± 0.48 N/mm for porcine tissue with an ultimate strain of 32.6 ± 13.6% for human tissue and a 43.3 ± 25.4% for porcine tissue. By making use of the average capsule thickness, an ultimate true stress was also determined for the capsule, 1.85 ± 1.18 MPa for human tissue and 2.03 ± 2.44 MPa for porcine tissue.

Although previous studies have provided insight into the mechanical response of liver parenchyma in tensile loading, they are limited by their use of animal tissue and quasi-static strain rates. To accurately predict liver lacerations in MVCs, the material response of human liver in tensile loading is needed. However, to the best of the author's knowledge there has been no previous attempt to quantify the viscoelastic response of human liver parenchyma in tensile loading. Therefore, the purpose of this study was to quantify the tensile mechanical properties of human liver parenchyma at four distinct strain rates varying from static, to quasistatic, to dynamic.

METHODS

A total of 51 uniaxial tension tests were performed on the parenchyma of 7 unembalmed human livers obtained from Post Mortem Human Subjects (PMHS). Each liver was obtained within 36 hours of death and tested within 48 hours of death. NDRI (National Disease Research Interchange Philadelphia, PA) and Wake Forest University Baptist Medical Center (Winston-Salem, NC) supplied the livers. Subject sex, age, weight, and height, were tabulated along with the time to procurement from death and time to test completion from death (Table 8). All subjects were screened for any medical issues that might affect the mechanical properties of the liver such as cancer in the abdomen or hepatitis. Livers were not frozen at any point during the

transportation, preparation, or testing processes because it was shown that freezing the tissue reduces the average failure strain by 49% (Santago et al. 2009b). All livers were immersed in Dulbecco's Modified Eagle's Medium (DMEM) prior to transportation and transported with wet ice.

Table 8: Subject Information

Liver	Origin	Sex	Age	Weight	Height	Procurement Time	Testing completed
		(M/F)	(years)	(kg)	(meters)	(hours post death)	(hours post death)
1	Wake	F	77	66	1.68	3	29
2	NDRI	M	78	N/A	N/A	10	29
3	NDRI	F	67	82	1.55	8	45
4	NDRI	F	57	66	1.73	11	39
5	NDRI	M	69	N/A	N/A	22	48
6	NDRI	F	80	N/A	N/A	11	45
7	NDRI	F	64	45	1.60	15	36

In order to test the parenchyma in uniaxial tension, "dog-bone" shaped tension samples were prepared. To create the samples, a constant thickness slice of the parenchyma was first obtained from the parenchyma of the liver. A custom blade assembly and slicing jig were utilized to create this slice (Figure 13). The blade assembly was constructed of multiple 48.3 cm long razor blades and spaced 5 mm apart by aluminum spacers. The slicing jig was constructed of aluminum U shaped pieces spaced 5 mm apart to act as guides for the blades. To obtain the tissue slices, a block of tissue was first cut from the parenchyma of the liver and placed in the slicing jig (Figure 14). The block dimensions were determined such that the block would fit securely in the slicing jig. The blades on the blade assembly were then aligned in the groves of the slicing jig. The slicing was performed with one smooth pass of the blades through the tissue block while minimizing downward force in order to avoid damaging or deforming the tissue. Multiple pieces of constant thickness liver parenchyma were obtained after each slicing pass. After slicing, the tissue samples were then immersed in a DMEM bath to maintain specimen hydration.

Figure 13: Custom made slicing jig (left) and blade assembly (right)

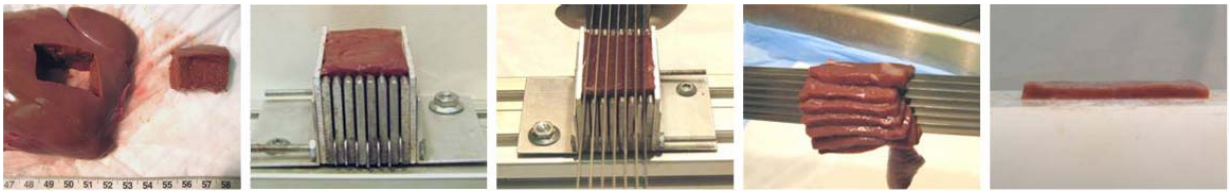

Figure 14: Tissue Slicing Methodology

To ensure that the dog-bone shaped tissue samples were consistent and would not fail at an inappropriate location, a custom stamp and stamping base were designed. The stamp was designed so that the stress concentrations were minimized in the fillet region so that failure would occur in the gage length (Figure 15). The stamp consisted of steel bent to the specified dimension and imbedded in wood (Figure 16). The edges of the steel were sharpened so that the specimen edges were not damaged. In order for the stamp to be consistently positioned on the stamping block and to constrain the stamp during tests, guide holes were drilled in the wooden block which corresponded to the locations of the guide rods on the stamping base (Figure 16).

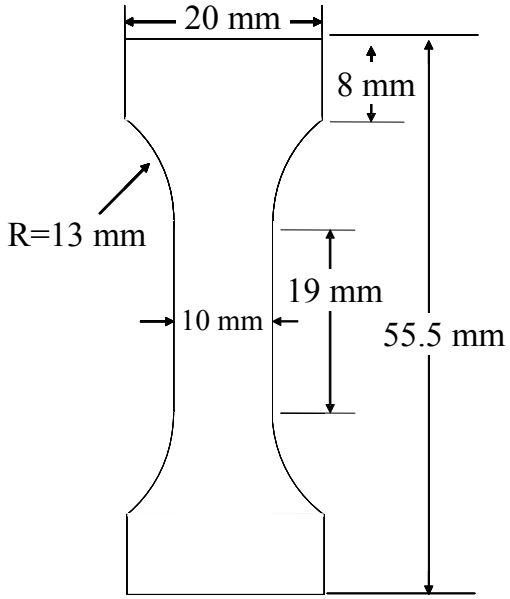

Figure 15: Dimensions of the specimen stamp

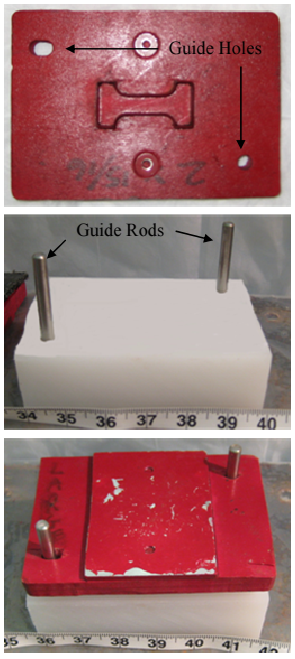

Figure 16: Stamp with associated stamping base

A slice of tissue was placed on the stamping base and positioned with the help of a cut out jig in order to obtain a specimen devoid of any visible vasculature or defects (Figure 17). The cut out jig had holes placed in it that corresponded to the guide rods on the stamping base so that the cut

out jig could be consistently aligned. Once the tissue sample was positioned, the stamp was placed on top of the tissue using the guide rods. Finally, a plastic block was placed on top of the stamp and lightly struck several times so that the stamp would cut the tissue into the desired shape. After stamping, the dog-bone specimens were immersed in a DMEM bath to maintain specimen hydration.

Figure 17: Specimen Stamping Methodology

Before the specimens were mounted and tested, they were heated to physiological temperature. A hot plate was used to heat the DMEM to approximately 37°C, and the tissue specimens were immersed in the heated fluid (Figure 18). The specimens were left in the heated DMEM for a minimum of six minutes before they were removed and mounted in the grip assembly. An environmental test chamber was constructed to house the testing equipment and allow the test environment to be heated to approximately 37°C (Figure 19). The frame of the environmental chamber was constructed with wood. Plastic was then stapled so to the wood so that the testing around was completely enclosed. Two space heaters were utilized to heat the space inside the structure and were controlled with a thermostat. A metal platform was utilized to block the heaters from blowing directly onto the testing apparatus.

Figure 18: The hot plate warms the tissue to approximately 37°C

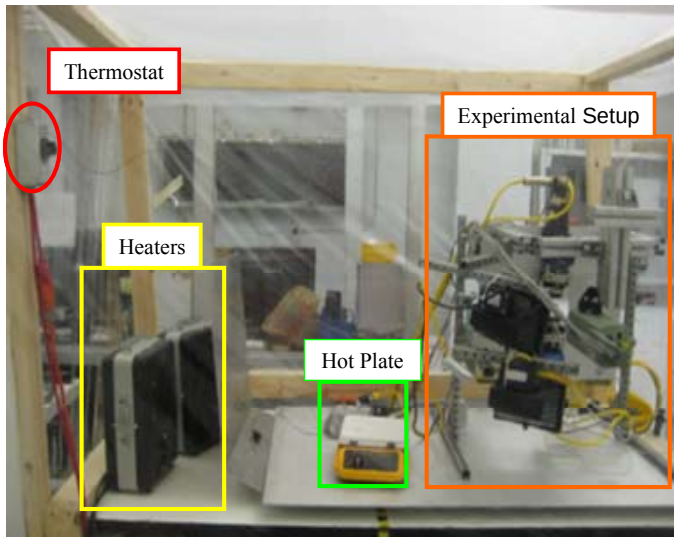

Figure 19: The thermostat controls the two heaters which heat the chamber while the hot plate warms the tissue

A custom testing apparatus, similar to the one utilized by Manogian (2008) was constructed with two linear motors attached to an vertical aluminum plate (Figure 20). The linear motors (Parker ViX, Irwin, PA) were controlled by one multi-axis controller (Parker ACR9000, Irwin, PA). Each stage was instrumented with a potentiometer (Space Age Control, 160-1705, 540mm, Palmdale, CA). An aluminum bar was connected to the motor which allowed a grip assembly to be rigidly attached using a set screw. Each of the two grip assemblies was instrumented with a load cell (Interface WMC-5, Scottsdale, AZ) and accelerometer (Endevco 7264B, 2000 G, San Juan Capistrano, CA). The multi-axis controller synchronized the grip movements which allowed each grip assembly to be moved at the same velocity and at the same time.

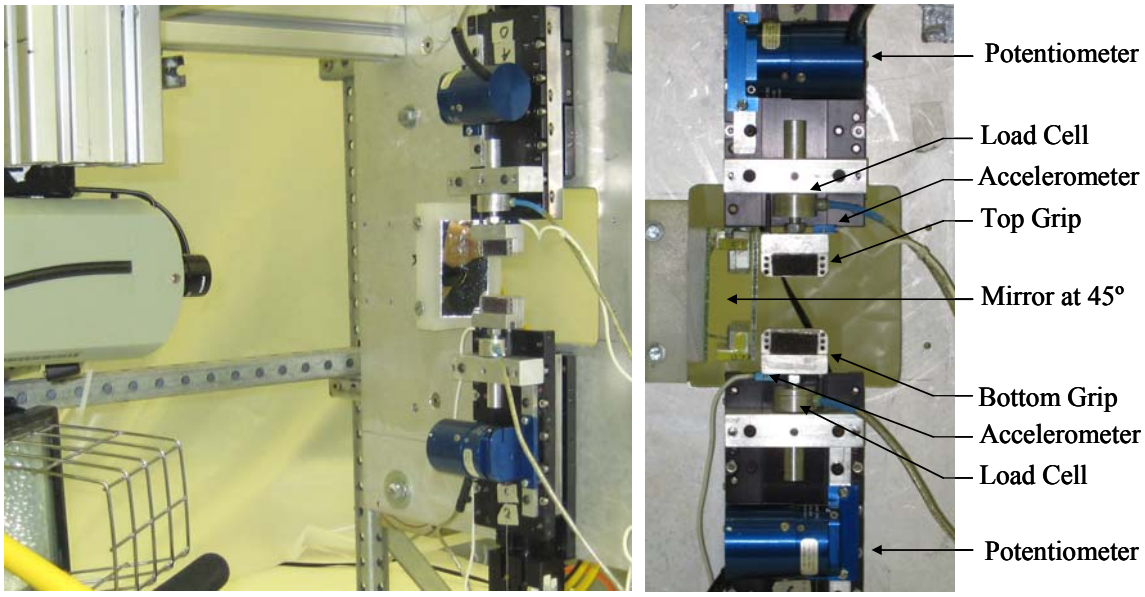

Figure 20: Experimental Setup

A detailed specimen mounting procedure was developed in order to minimize the confounding affects of shear due to improper specimen alignment, and to minimize variations in initial conditions between the specimens (Figure 21). Initially, the top grip assembly was removed from the testing apparatus and laid flat. The specimen was placed on the top grip in such a way that its main axis was aligned with the centerline of the load cell. A clamping piece was then placed on top of the tissue and was attached to the top grip assembly using screws. Sandpaper was adhered to the clamping piece and top grip assembly to keep the specimen from slipping from the grip during the loading process. The top grip assembly was then mounted in the test setup using a set screw and aligned so that the specimen was centered in view of the high-speed camera. The specimen was then allowed to hang in 1g of tension. The bottom grip assembly was placed in the testing apparatus and brought into position. The bottom of the tissue sample was then clamped into place using the same clamping mechanism described for the top grip. Special care was taken ensure that there was no slack in the tissue so that the 1g initial condition was maintained.

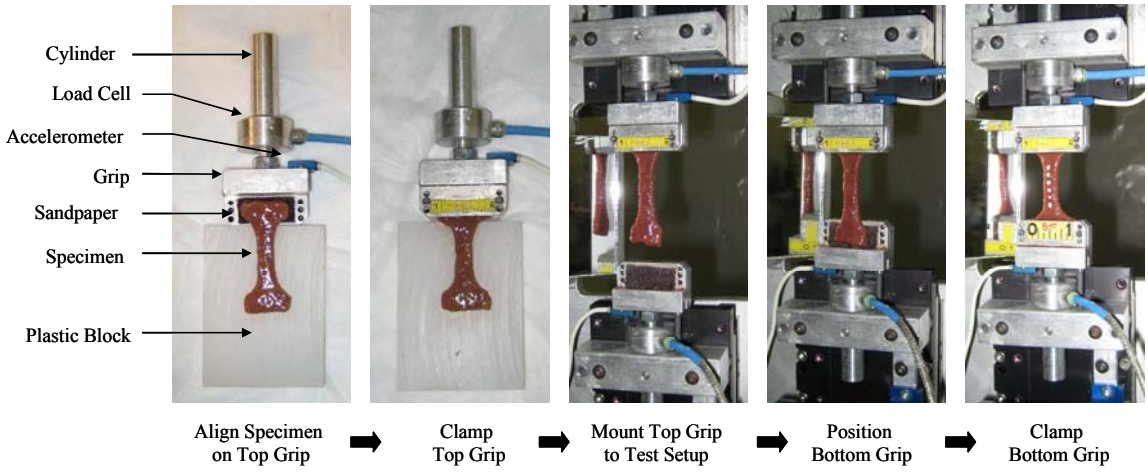

Figure 21: Specimen Mounting Methodology

Once the specimens were mounted, posterior and lateral pretest pictures were taken with high resolution digital cameras, 370 pixels/in and 350 pixels/in respectively, in order to obtain initial width and thickness measurements (Figure 22). To investigate rate dependence, each specimen was pulled to failure at one of the four desired strain rates: 0.01 s^{-1}, 0.10 s^{-1}, 1.00 s^{-1}, and 10.00 s^{-1}. A high-speed video camera (Phantom V4, Vision Research, Wayne, NJ) was used to obtain localized deformation throughout the duration of the test and failure time. Camera resolution was 512 pixels x 512 pixels, resulting in an approximate resolution of 7.7 pixels/mm. Once the specimens had been mounted, equally spaced markers were placed on the gage length in view of the camera. Sampling rates used to acquire load cell data, accelerometer data, and high-speed video are reported in Table 9.

Table 9: Data Acquisition and High-Speed Video Sampling Rates by Loading Rate

Rate	Desired Strain Rate (s^{-1})	Data Acquisition (kHz)	High-Speed Video (Frames/sec)
Rate 1	0.01	0.2	20
Rate 2	0.10	2.0	70
Rate 3	1.00	20.0	500
Rate 4	10.00	40.0	100

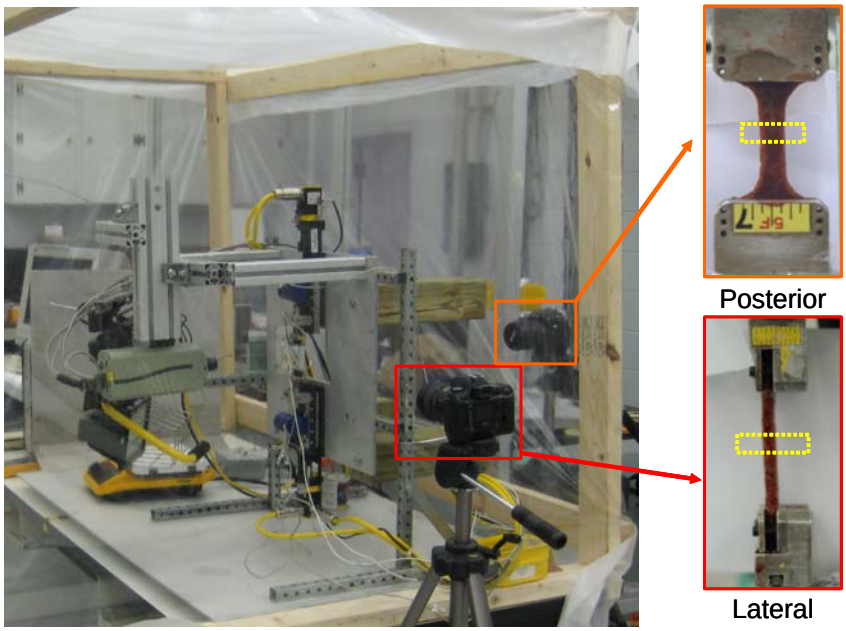

Figure 22: Location of Cameras and Typical Pre Test Posterior and Lateral Images

Before the test could be deemed acceptable, the high-speed video was analyzed to determine if the criteria for an acceptable test was met. To meet the criteria, the specimen must have torn in the gage length, not have any noticeable deformities or abnormalities, and not have pulled out of either grip. Failure time was defined as the point in which the failure tear initiated in the high speed video. If the initiation of the failure tear could not be observed in the video, then failure was defined as the point of peak load preceding a significant decrease in load.

Once failure time had been determined, the optical markers placed on the tissue were tracked throughout the duration of the test using TEMA® Advanced Motion Analysis Software (Linköping, Sweden) to determine failure strain. Two optical markers were chosen, one either side of the failure tear, and their relative displacement was tabulated throughout the duration of the test. To obtain a more localized failure strain, markers were chosen based on their proximity to the failure tear with markers closest to the failure tear beginning chosen first. However, in certain situations, the failure tear was through a marker or edge of a marker; therefore, the next closest marker on the same side of the failure tear was chosen. The resulting displacement was then cut at the failure time. Next, the cut data was input into an original Matlab code and curve fit using a 5^{th} degree polynomial (Manoogian et al. 2008). The average R^2 value for the displacement curve fit was 0.997 ± 0.005. Resulting curve fitt data was analyzed to determine

Green-Lagrangian Strain (ϵ) using the instantaneous distance between two markers (L_n), the original distance between the same two markers (L_o), and the stretch ratio (λ) (eq. 7, eq. 8). Strain rate was determined by calculating the slope of the strain versus time curve between 25% and 75% of the maximum strain value.

$$\lambda = \frac{L_n}{L_o} \quad \textbf{eq. 7}$$

$$\varepsilon = \frac{1}{2}\left(\lambda^2 - 1\right) \quad \textbf{eq. 8}$$

An analysis was performed to determine error in the TEMA tracking data. A fixed distance was tracked during the duration of three randomly chosen tests from each rate. Distance between the fixed points was determined for each instant in time. The maximum deviation from the mean value was determined for each test and averaged. This resulted is an average maximum tracking error of 0.69 pixels, which corresponds to approximately 0.09 mm. Similar TEMA tracking for tensile tests has been previously reported (Manoogian et al. 2008).

In order to calculate stress, the raw force (F) data must be inertially compensated (F_{IC}) (eq. 9). The effective mass (m) was multiplied by the acceleration (a) and this value was subtracted from the raw force seen by the load cell (F). Effective mass was defined as ½ the load cell mass plus the mass between the load cell and the specimen. Inertially compensated force was then down sampled and cut at the failure time. Cut force data was curve fit with a 5^{th} degree polynomial (Manoogian et al. 2008). The average R^2 value for the force curve fit was 0.977±0.044.

Initial area at the location of the failure tear was then determined. The high-speed video was analyzed to determine the pretest location from which the failure tear propagates. A pretest distance from one grip to the failure location was established, and this information was utilized to determine the original width and thickness from the pretest pictures (Figure 22). The error for the picture measurements is ±2 pixels. Given the instantaneous force from the curve fit force data (F_c), the cross-section area (A_o) determined from the original width and thickness, and the instantaneous stretch ratio (λ), 2^{nd} Piola Kirchhoff Stress (S) was tabulated (eq. 10). Characteristic 2^{nd} Piola Kirchhoff Stress vs. Green-Lagrangian strain curves were determined for

all rates using a standard method (Lessley et al. 2004). Average and standard deviation of failure stress, failure strain, and actual strain rate were tabulated for each desired strain rate. A series of two-tailed Student's t-tests for means, assuming unequal variance, were performed to determine if there were statistically significant differences in failure stress and failure strain between each loading rate. Significance was defined as a two-tailed p-value of ≤ 0.05.

$$F_{IC} = F - m * a \quad \textbf{eq. 9}$$

$$S = \frac{F_C}{\lambda * A_o} \quad \textbf{eq. 10}$$

RESULTS

A total of 51 uniaxial failure tensile tests were performed on the parenchyma of human liver. All rates showed a non-linear characteristic stress versus strain response. Failure occurred in the gage length of each specimen (Figure 23). Stress versus strain curves for the uniaxial tension tests are shown below (Figure 24 - Figure 27). The data are reported as 2nd Piola Kirchhoff Stress and Green-Lagrangian Strain. A total of 47 tests were performed at Rate 1 with 16 of them being acceptable. The desired strain rate for Rate 1 was 0.01 s^{-1}; however, the average strain rate for Rate 1 was 0.008 ±0.001 s^{-1}. The stress versus strain data for each test performed at Rate 1 is plotted along with the corresponding characteristic average and standard deviations for failure stress and strain (Figure 24). The average failure stress and strain were 40.21 ± 21.39 kPa and 0.34 ± 0.12, respectively. A total of 46 tests were performed at Rate 2 with 11 of them being acceptable. The desired strain rate for Rate 2 was 0.1 s^{-1}; however, average strain rate for Rate 2 was 0.089 ± 0.014 s^{-1}. For Rate 2 each tests stress versus strain data and the corresponding characteristic average and standard deviations for failure stress and strain are shown in Figure 25. The average failure stress and strain were 46.79 ± 24.81 kPa and 0.32 ± 0.05, respectively. A total of 43 tests were performed at Rate 3 with 12 of them being acceptable. The desired strain rate for Rate 3 was 1.0 s^{-1}; however, average strain rate for Rate 3 was 0.871 ± 0.093 s^{-1}. Stress versus strain data for each Rate 3 test is plotted along with the corresponding characteristic average and standard deviations for failure stress and strain (Figure 26). The average failure stress and strain were 52.61 ± 25.73 kPa and 0.30 ± 0.10, respectively. A total of 45 tests were performed at Rate 4 with 12 of them being acceptable. The desired strain rate for Rate 4 was 10.0

s^{-1}; however, the average strain rate for Rate 4 was 9.524 ± 1.964 s^{-1}. For Rate 4 each tests stress versus strain data and the corresponding characteristic average and standard deviations for the failure stress and strain are shown in Figure 27. The average failure stress and strain were 61.02 ± 24.89 kPa and 0.24 ± 0.07, respectively. The success rate for an acceptable test, for all tests combined, was 28%. The characteristic average stress vs. strain for each rate was plotted so that a clear comparison could be made (Figure 28). P-values for all comparisons have been tabulated (Table 10). Bold values are significant.

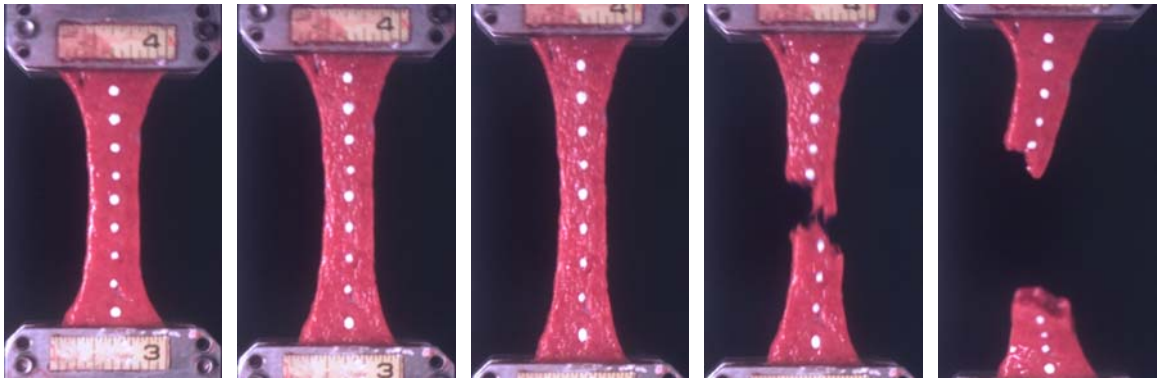

Figure 23: High-Speed Video Stills of a Typical Uniaxial Tension Test

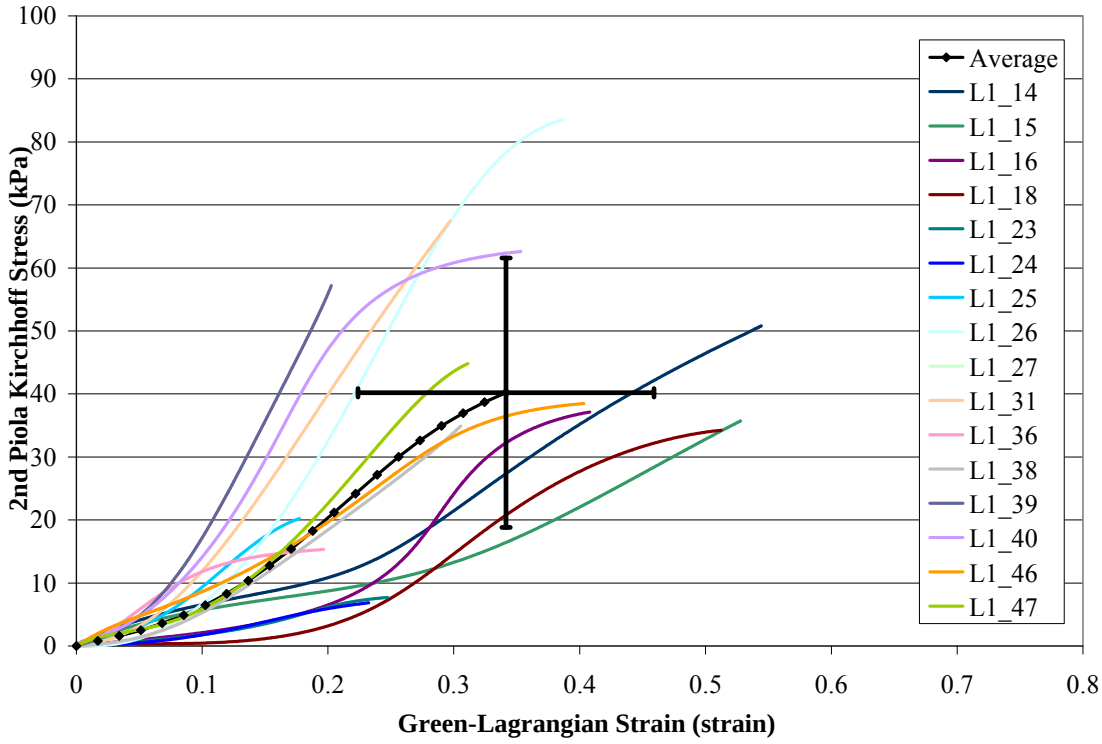

Figure 24: Stress vs. Strain data for the tests conducted at 0.008 s^{-1} and associated characteristic average

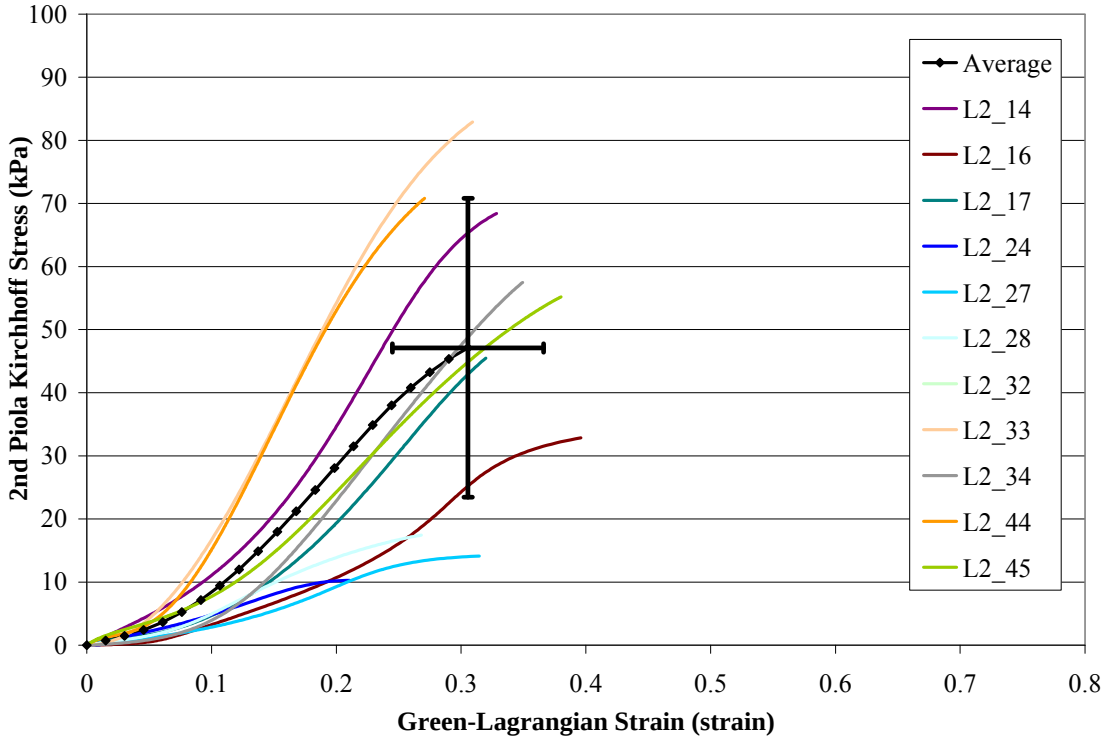

Figure 25: Stress vs. Strain data for tests conducted at 0.089 s^{-1} and associated characteristic average

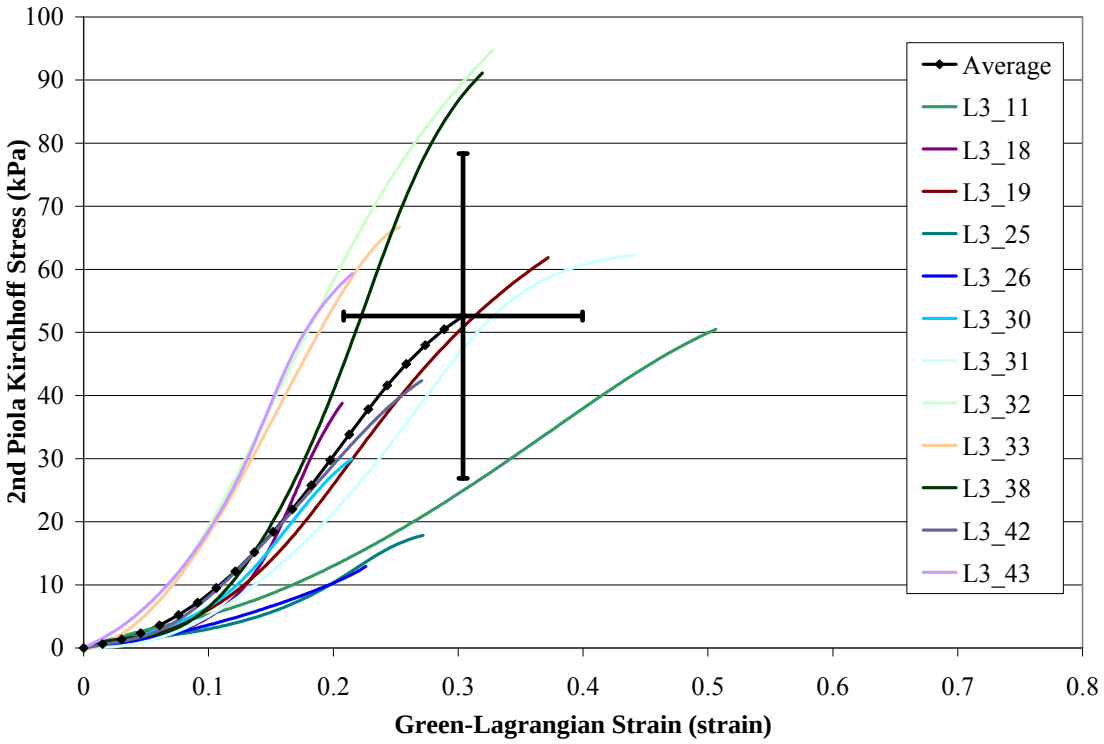

Figure 26: Stress vs. Strain data for tests conducted at 0.871 s^{-1} and associated characteristic average

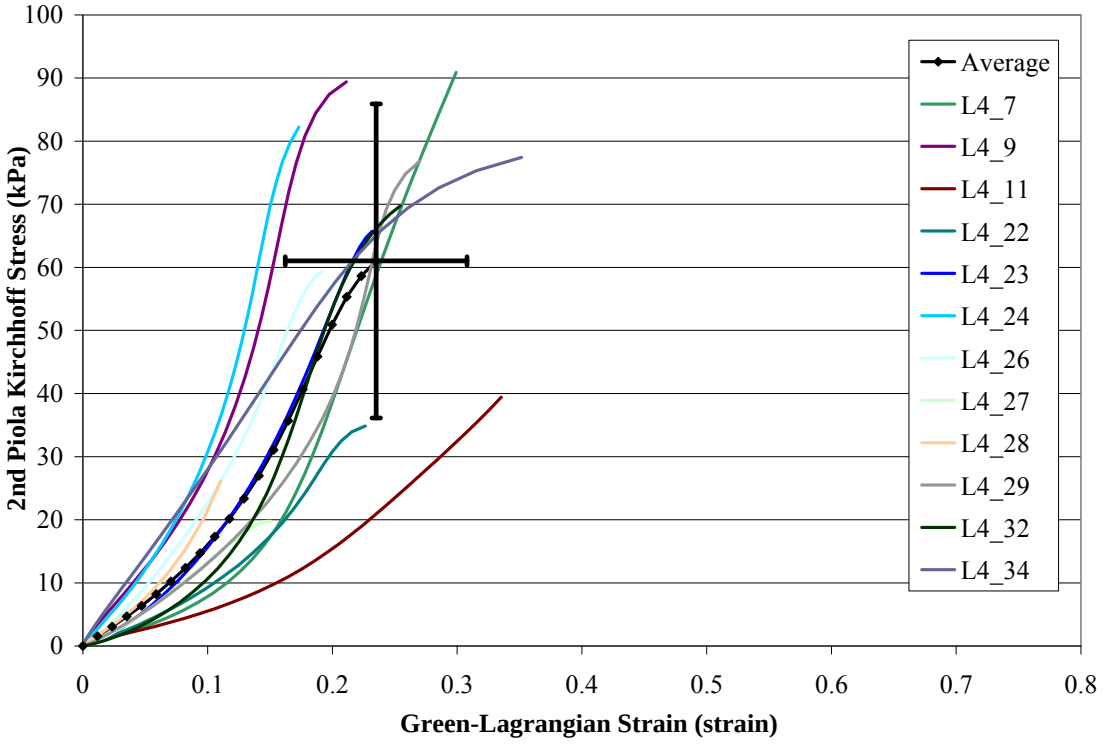

Figure 27: Stress vs. Strain data for tests conducted at 9.524 s^{-1} and associated characteristic average

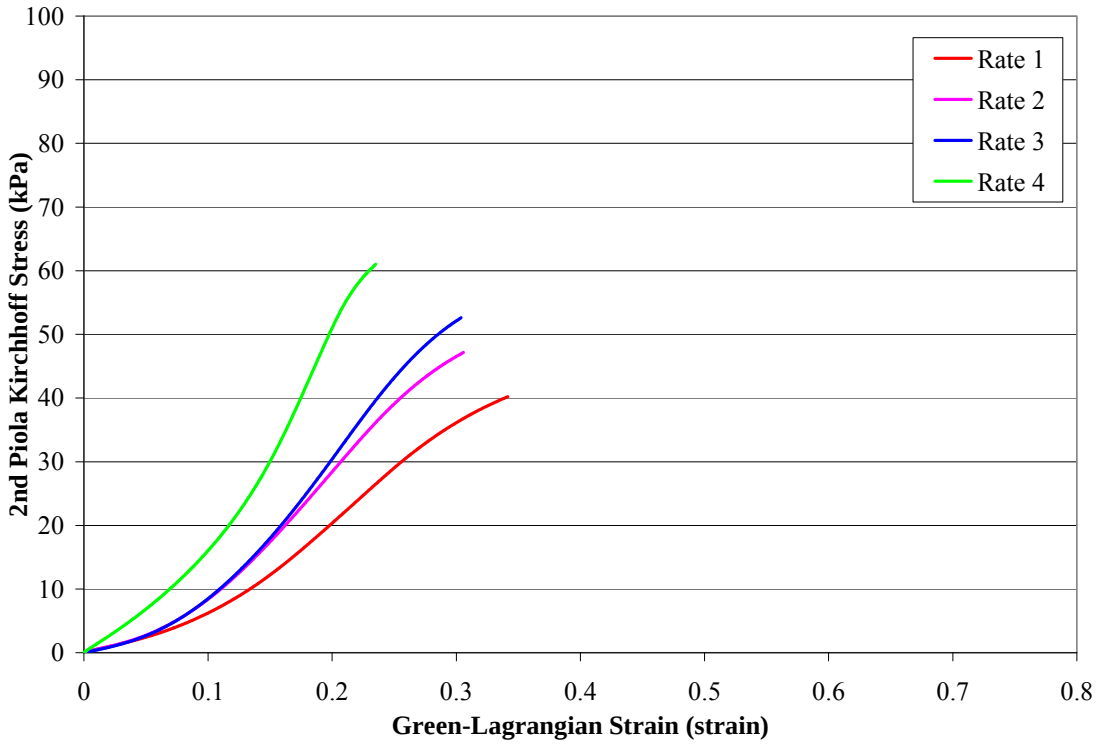

Figure 28: Characteristic Averages for Each Rate

Table 10: Two-tailed Student-t-test p-values for comparisons made in between each loading rate.

Comparison	Strain	Stress
	p-value	p-value
Rate 1 to Rate 2	0.50	0.47
Rate 1 to Rate 3	0.37	0.18
Rate 1 to Rate 4	**0.01**	**0.03**
Rate 2 to Rate 3	0.72	0.59
Rate 2 to Rate 4	**0.01**	0.18
Rate 3 to Rate 4	0.06	0.42

DISCUSSION

This study is the first to present stress versus strain data and failure information for the parenchyma of human liver at static, quasistatic, and dynamic loading rates. Most of the variance seen in the data can be attributed to specimen variability since all of the specimens were prepared and tested in an identical way. Although the parenchyma has some irregularities, special care

was taken to avoid these during the stamping procedure. However, the existence of small non-visible vasculature inside the tissue samples is unavoidable and could contribute to the specimen variation.

It was determined, from these tests, that the human liver has some rate dependence properties. Although statistical significance was only seen in between Rate 1 and Rate 4 from average failure stress, statistical significance was seen in between Rate 1 and Rate 4 and Rate 2 and Rate 4 for average failure strain. Failure stress did increase and failure strain did decrease with increasing strain rate. These results correspond with previous studies (Uehara 1995).

Although there have been no previous studies testing human liver parenchyma in uniaxial tension, failure properties of porcine, bovine, and rabbit liver parenchyma developed from tension tests have been reported (Santago et al. 2009a; Santago et al. 2009b; Uehara 1995; Yamada 1970). Before a direct comparison could be made between the porcine data from Uehara (1995) and the current study, the data from the current study needed to be converted to true stress and nominal strain. This was performed by assuming a poisons ratio of 0.5. A strain rate was calculated for the porcine data by dividing the reported strain velocity by the reported average initial length of the specimen. It was then determined that the porcine stress and strain values determined from tests conducted at 20mm/min and at 200mm/min were comparable to stress and strain values determined from human tests conducted at Rate 1 and Rate 2 respectively (Figure 29, Figure 30). Although the strain values are almost identical, the stress values differ significantly. This discrepancy can be explained by the difference in cellular structure between porcine and human liver. The lobule is the functional unit of the liver (Guyton and Hall 2006). The lobule has a cylindrical shape with central vein passing through its core surrounded by radiating sheets of hepatocyte cells (Saladin and McFarland 2008). It has been previously shown that human liver parenchyma has a similar lobule to that of porcine liver parenchyma; however, the thin septa of collagenous supporting tissue seen in the porcine liver parenchyma is absent in the human liver parenchyma (Burkitt et al. 1993). It has also been previously demonstrated that, as the percentage of connective tissue content increases, the stiffness increases (Mazza et al. 2007). Because the porcine liver has a larger amount of connective tissue than the human liver, failure stress for porcine liver parenchyma would be higher. However, the connective tissue

inside either liver is not aligned in any particular direction because it surrounds the lobule (Saladin and McFarland 2008); therefore, increasing the amount of connective tissue would not significantly increase failure strain.

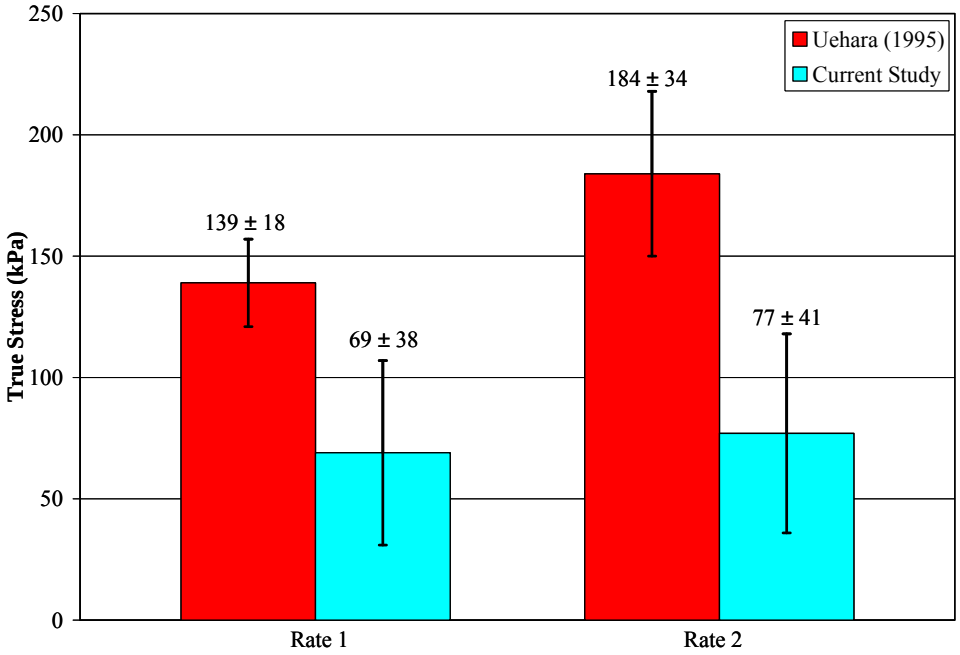

Figure 29: Failure Stress Comparison between Uehara (1995) and Current Study

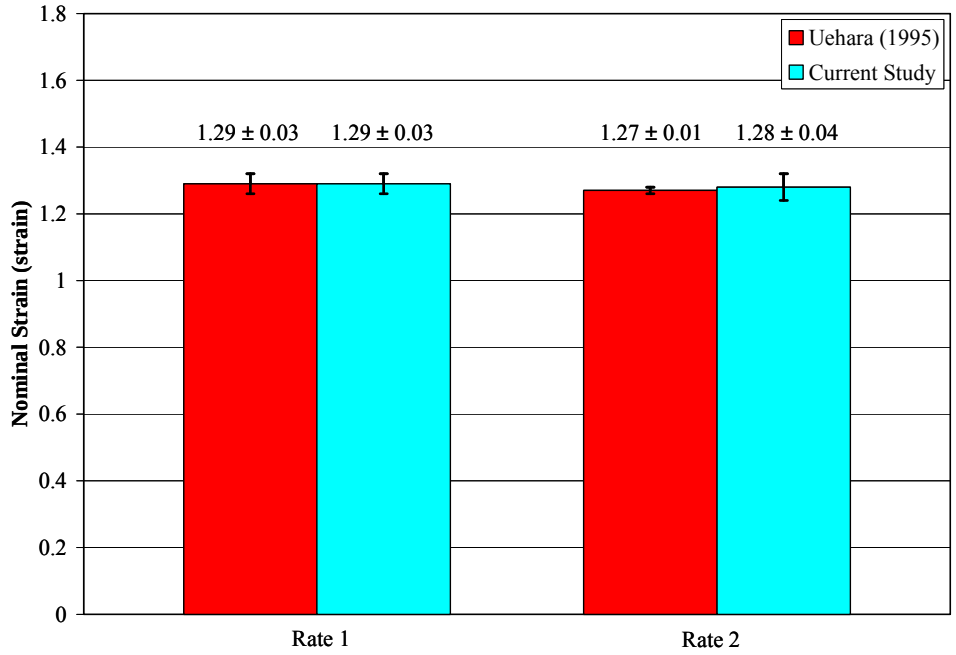

Figure 30: Failure Strain Comparison between Uehara (1995) and Current Study

There have been a total of 32 uniaxial tensile tests on the parenchyma of bovine liver obtained from 3 livers that are comparable to tests conducted at Rate 3 in the current study (Santago et al. 2009a; Santago et al. 2009b). The data has been tabulated below for comparison (Figure 31, Figure 32). Average failure strain matches well for all livers; however, the average failure stress for each bovine liver does not compare well to the average failure stress of the human livers. Average human failure stress from the current study has been determined from a number of livers and therefore has a large range (13 kPa to 95 kPa). To make a direct comparison, all bovine data needs to be combined. When this is done, the average failure stress and the range (11 kPa to 101 kPa) is comparable to that of the human average failure stress and range. Similar to human liver parenchyma, bovine liver parenchyma contains less connective tissue than porcine liver tissue and the connective tissue does not online the lobules as seen porcine liver parenchyma (Dyce et al. 2002a; Dyce et al. 2002b). Data on the mechanical properties of rabbit liver can be not directly compared to the current study because the strain rate is unknown.

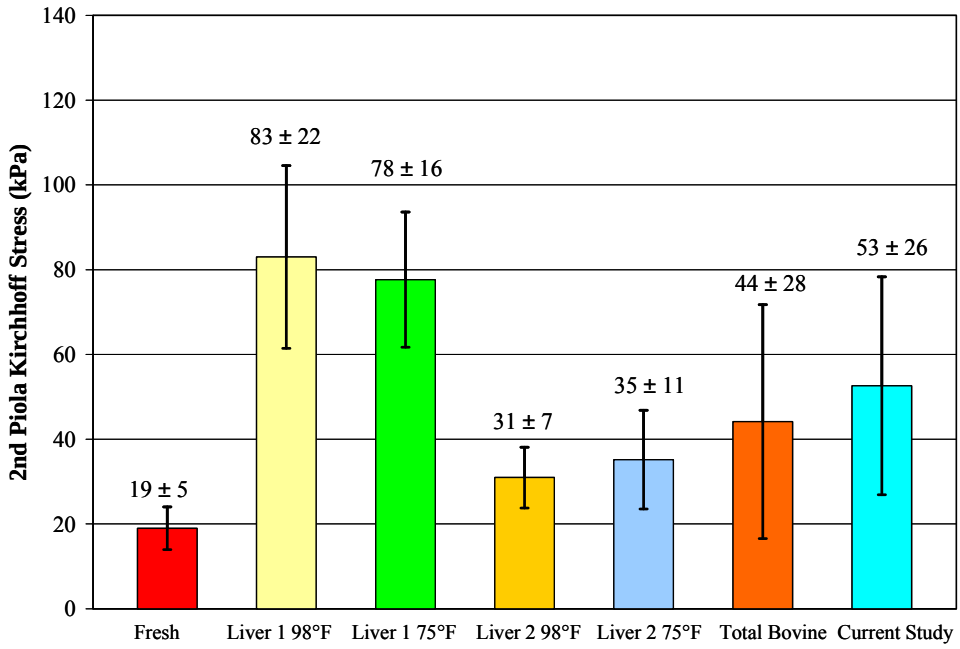

Figure 31: Comparison of Failure Stress between Bovine Data and Current Study at Rate 3

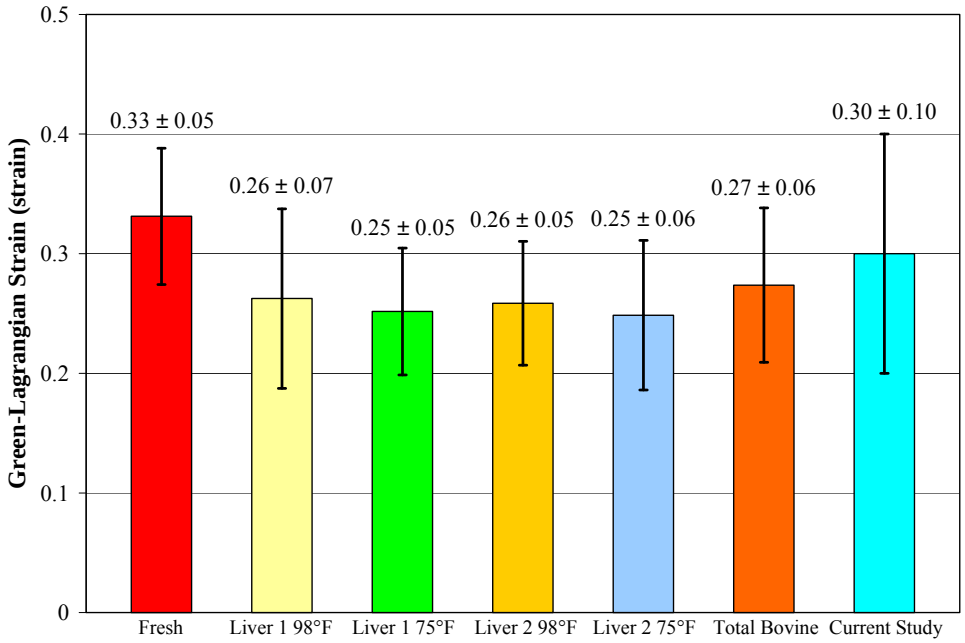

Figure 32: Comparison of Failure Strain between Bovine Data and Current Study at Rate 3

Uniaxial tension tests have also been performed on specimens from human and porcine livers that combined parenchyma and capsule (Brunon et al. 2010). Tests conducted on the combined parenchyma and capsule samples had strain rates between 0.001 s^{-1} and 0.01 $s^{-1,}$ which are comparable to the tests performed at Rate 1 and Rate 2 in the current study. To compare the data, force per unit width was tabulated for each of the tests in the current study assuming a Poison's ratio of 0.5. A 0.2 N load was utilized by Brunon et al. (2010) to overcome an initial state of compression described by Gao and Desai (2010). To account for this, the data in the current study was shifted to allow for a comparison. The specimens tested by Brunon et al. (2010) had similar failure stress values to those measured in the current study (Figure 33). However, failure strain in the current study is significantly less than that measured by Brunon et al (2010) (Figure 34). This can be explained by the specimen mounting procedure utilized in the different studies. Brunon et al. (2010) placed their specimens in the clamps and then placed the clamps into the testing apparatus. This would result in an initial state of compression. In the current study, each specimen was allowed to hang under its own weight before being clamped in the bottom grip. This process would rid the sample of any initial compressive state; therefore, the 0.2 N shift is not needed. When comparing the nonshifted data from the current study to Brunon et al (2010)

the average failure strains are similar. Similar to Uehara (1995), the porcine load per unit width value was significantly higher than the value from the current study while the strain values were comparable.

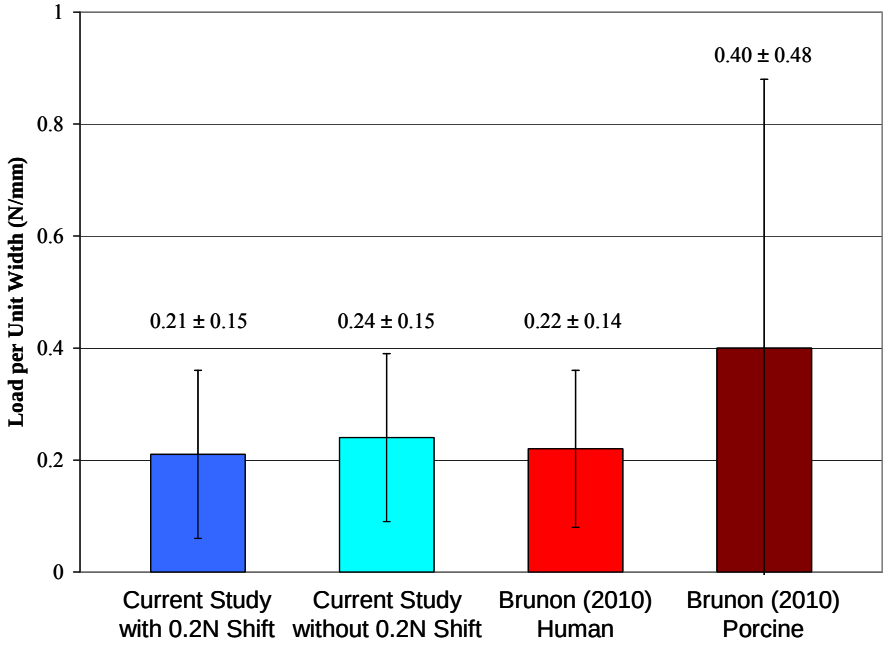

Figure 33: Comparison of Failure Load per Unit Width between Brunon (2010) and Current Study

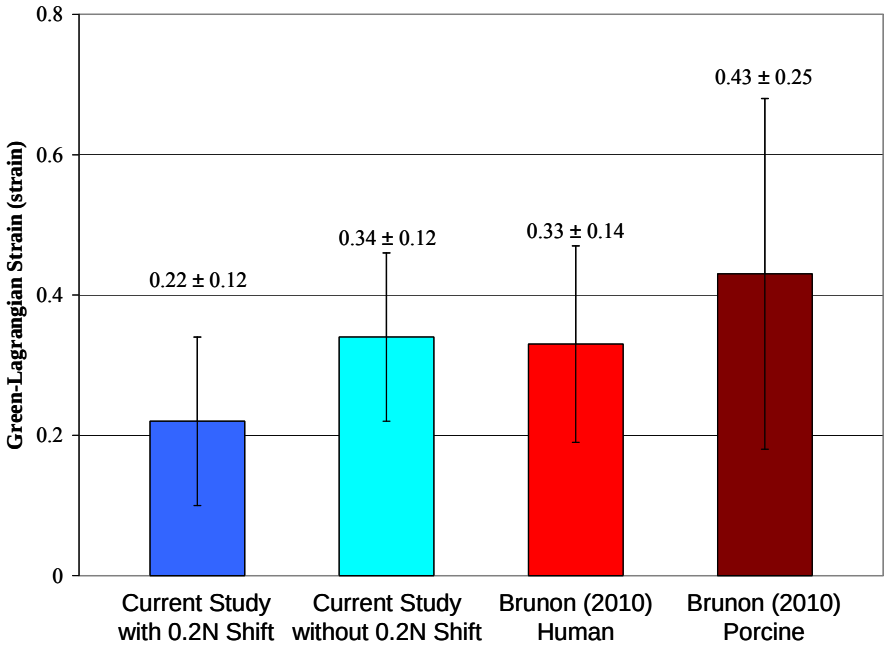

Figure 34: Comparison of Failure Strain between Brunon (2010) and Current Study

Hollenstein et al (2006) conducted tests on isolated human liver capsule at 0.005 s^{-1}, which compares to the tests conducted at Rate 1 in the current study (Table 11). A 0.2N pre load was applied to the sample before the failure test was performed; however, the data in the current study was not shifted to reflect this because of the explanation given above. However, nominal stress and nominal strain were reported by Hollenstein et al. (2006) so the data in the current study was converted to this type of stress and strain. It can be seen that the bovine liver capsule has higher failure stress and strain than that of the human parenchyma measured in the current study.

Table 11: Comparison of Tension Test Performed on Human Liver Parenchyma to Tension Tests Performed on Human Liver Capsule

Test	Nominal Stress (MPa)	Nominal Strain
Current (Human Liver Parenchyma)	0.07 ± 0.04	1.29 ± 0.09
Hollenstein (2006) (Human Liver Capsule)	9.20 ± 0.70	1.36 ± 0.05

The comparison of the current study to previous studies involving animal tissue (Hollenstein et al. 2006; Santago et al. 2009a; Santago et al. 2009b; Uehara 1995) demonstrates that differences in cellular structure between animal and human liver tissue can result in significant differences in the material response. In addition, the differences between animal and human liver varies with respect to species of the animal.

There are limitations with this study. A total of 27% of the resting cardiac output flows through the liver each min (Guyton and Hall 2006). In order to take this into consideration, the samples were kept saturated in DMEM prior to testing. However, blood flow and pressure *in vivo* were not taken into consideration. Warm ischemia time for each subject is also unknown and has been shown to negatively affect initial graft function during transplants (Platz et al. 1997). Post mortem procurement time and post mortem test completion time vary widely. These factors could contribute to tissue degradation, thereby affecting the biomechanical properties of the liver tissue.

CONCLUSION

This study presented a total of 51 uniaxial tensile tests on the parenchyma of human liver. A total of 7 livers were utilized to acquire dog-bone shaped specimens for testing. Material properties of

human liver parenchyma were evaluated at four average strain rates: 0.008 s^{-1}, 0.089 s^{-1}, 0.871 s^{-1}, and 9.524 s^{-1}. Failure stresses of 40.21 ± 21.39 kPa, 46.79 ± 24.81 kPa, 52.61 ± 25.73 kPa, and 61.02 ± 24.89 kPa were seen for each rate respectively. Failure strains of 0.34 ± 0.12, 0.32 ± 0.05, 0.30 ± 0.10, and 0.24 ± 0.07 were seen for each rate respectively. Statically significant rate dependence is seen in between Rate 1 and Rate 4 for average failure stress. However, rate significance was seen between Rate 1 and Rate 4 and between Rate 2 and Rate 4 for average failure strain. When compared to previous tensile liver tests, the current study addresses the material response to strictly the human liver parenchyma as well as addresses the need for dynamic loading rates. In summary, failure tensile material properties for the parenchyma of the human liver have been discovered at static, quasistatic, and dynamic loading rates for use as material properties and injury tolerance values to create finite element models.

ACKNOWLEDGEMENTS

The author would like to acknowledge the Toyota Motor Corporation for their funding and support.

REFERENCES

Augenstein JS, Bowen J, Perdeck EB, Singer M, Stratton JE, Horton T, Rao A, Digges KH, Malliaris AC, Steps J. 2000. Injury patterns in near-side collisions. SAE 2000 World Congress: SAE International.

Bondy N. 1980. Abdominal Injuries in the National Crash Severity Study. National Center for Statistics and Analysis. 59-80 p.

Brunon A, Bruyere-Garnier K, Coret M. 2010. Mechanical characterization of liver capsule through uniaxial quasistatic tensile tests until failure. Journal of Biomechanics:10.1016/j.jbiomech.2010.03.038

Burkitt HG, Young B, Heath JW. 1993. Liver and pancreas. Wheater's Functional Histology: A Text and Colour Atlas. 3rd ed. New York: Churchhill Livingstong. p 272-277.

Christmas AB, Wilson AK, Manning B, Franklin GA, Miller FB, Richardson JD, Rodriquez JL. 2005. Selective managment of blunt hepatic injuries including nonoperative management is a safe and effective strategy. Surgery 138(4):606-610.

Dyce KM, Sack WO, Wensing CJG. 2002a. The Abdomen of the Pig. Textbook of Veterinary Anatomy. 3rd ed. Philadelphia: Saunders. p 781-782.

Dyce KM, Sack WO, Wensing CJG. 2002b. The Abdomen of the Ruminants. Textbook of Veterinary Anatomy. 3rd ed. Philadelphia: Saunders. p 685-686.

Elhagediab AM, Rouhana SW. Patterns of Abdominal Injury in Frontal Automotive Crashes; 1998; Windsor, Ontario, Canada.

Gao Z, Desai JP. 2010. Estimating zero-strain states of very soft tissue under gravity loading using digital image correlation. Medical Image Analysis 14(2):126-137.

Guyton AC, Hall JE. 2006. Textbook of Medical Physiology. New Delhi, India: Elsevier. 1116 p.
Holbrook TL, Hoyt DB, Eastmen AB, Sise MJ, Kennedy F, Velky T, Conroy C, Pacyna S, Erwin S. 2007. The Impact of Safety Belt Use on Liver Injuries in Motor Vehicle Crashes: The Importance of Motor Vehicle Safety Systems. Journal of Trauma 63(2):300-306.
Hollenstein M, Nava A, Valtorta D, Snedeker JG, Mazza E. 2006. Mechanical Characterization of the Liver Capsule and Parenchyma. In: Szekely MHG, editor. Biomedical Simulation. Berlin/Heidelberg: Springer-Verlag. p 150-158.
Hurtuk M, Reed RLI, Esposito TJ, Davis KA, Luchette FA. 2006. Trauma surgeons practice what the preach: The NTDB story on solid organ injury management. Journal of Trauma 61(2):243-255.
John TG, Greig JD, Johnstone AJ, Garden OJ. 1992. Liver Trauma: A 10-year experience. British Journal of Surgery 79(12):1352-1356.
Kerdok AE, Ottensmeyer MP, Howe RD. 2006. Effects of perfusion on the viscoelastic characteristics of liver. Journal of Biomechanics(39):2221-2231.
Lessley D, Crandall J, Shaw G, Funk J, Kent R. 2004. A Normalization Technique for Developing Corridors from Individual Subject Responses. SAE Technial Paper Series. Detriot, MI.
Manoogian SJ, Bisplinghoff JA, McNally C, Kemper AR, Santago AC, Duma SM. 2008. Dynamic tensile properties of human placenta. Journal of Biomechanics 41(16):3436-3440.
Mazza E, Nava A, Hahnloser D, Jochum W, Bajka M. 2007. The mechanical response of human liver and its relation to histology: An in vivo study. Medical Image analysis 11(6):663-672.
Melvin JW, Stalnaker RL, Roberts VL, Trollope ML. Impact Injury Mechanisms in Abdominal Organs; 1973; Oklahoma City, OK. SAE. p 115-126.
Platz KP, Mueller AR, Schafer C, Jahns S, Guckelberger O, Neuhaus P. 1997. Influence of Warm Ischemia Time on Initial Graft Function in Human Live Transport. Transplantation Proceedings 29(8):3458-3459.
Saladin KS, McFarland RK. 2008. Human Anatomy 2nd Edition. 771 p.
Santago AC, Kemper AR, McNally C, Sparks JL, Duma SM. 2009a. The effect of temperature on the mechanical properties of bovine liver - biomed 2009. Biomed Sci Instrum 45:376-81.
Santago AC, Kemper AR, McNally C, Sparks JL, Duma SM. 2009b. Freezing affects the mechanical properties of bovine liver - biomed 2009. Biomed Sci Instrum 45:24-9.
Sparks JL, Bolte IV JH, Dupaix RB, Jones KH, Steinberg SM, Herriott R, Stammen J, Donnelly B. 2007. Using Pressure to Predict Liver Injury Risk from Blunt Impact. Stapp Car Crash J. p 401-432.
Stingl J, Baca V, Cech P, Kovanda J, Kovandova H, Mandys V, Rejmontova J, Sosna B. 2002. Morphology and some biomechanical properties of human liver and spleen. Surgical and Radiological Anatomy 24(5):285-289.
Tamura A, Omori K, Miki K, Lee JB, Yang KH, King AI. 2002. Mechanical characterization of porcine abdominal organs. Stapp Car Crash J 46:55-69.
Thor CP. 2008. Characteristics of Thoracic Organ Injuries in Frontal Crashes. Blacksburg: Virginia Polytechnic Institute and State University.

Uehara H. 1995. A study on the mechanical properties of the kidney, liver, and spleen, by means of tensile stress test with variable strain velocity. Journal of Kyoto Prefectural University of Medicine 104(1):439-451.
Wang BC, Wang GR, Yan DH, Liu YP. 1992. An Experimental Study on Biomechanical Properties of Hepatic Tissue Using a New Measuring Method. Bio-Medical Materials and Engineering 2:133-138.
Yamada H. 1970. Strength of Biological Materials. Baltimore: The Williams and Wilkins Company.

CHAPTER 4

EFFECT OF STRAIN RATE ON THE BIOMECHANICAL RESPONSE OF HUMAN LIVER TESTED IN UNCONFINED COMPRESSION

ABSTRACT

Motor vehicle collisions can result in life threatening liver injuries. Dummies are utilized to study injury in motor vehicle collisions; however, no crash test dummies are currently equipped to represent individual solid organs. This has increased the use of finite element models to help reduce these injuries; however, accurate material models need to be established to have accurate injury assessment using these models. This study presents a total of 36 unconfined compression tests on human liver parenchyma. A total of 6 livers were utilized to acquire cylindrically shaped compression samples for testing at four distinct strain rates: 0.008 s^{-1}, 0.074 s^{-1}, 0.776 s^{-1}, and 8.011 s^{-1}. All tests were performed within 48 hours of death. Force and displacement were determined from the impacting surface. Engineering stress and engineering strain were tabulated for each test. Rate dependence was seen with failure stress increasing and failure strain decreasing with increasing strain rate. Average failure stress ranged from -165 to -203 kPa while average failure strain ranged from -46% to -61%. This study provides failure compressive material properties for human liver parenchyma at static, quasistatic, and dynamic loading rates for use as material properties and injury tolerance values to create finite element models.

INTRODUCTION

Although injuries to the abdomen account for only 3-5% of all injuries in motor vehicle collisions (MVCs), abdominal injuries constitute 8% of AIS 3+, 16.5% of AIS 4+, and 20.5% of AIS 5+ injuries (Augenstein et al. 2000; Bondy 1980; Elhagediab and Rouhana 1998). The most frequently injured abdominal organ in MVCs is the liver, which accounts for approximately 38% of all abdominal injuries (Elhagediab and Rouhana 1998). The mortality rate for blunt liver injuries ranges from 9-17% but can be as high as 67% if the inferior vena cava or the hepatic veins are involved (Christmas et al. 2005; Hurtuk et al. 2006; John et al. 1992). Similarly, Holbrook et al. (2007) utilized the Crash Injury Research and Engineering Network (CIREN) to analyze liver injuries and determined that 47% of all liver injuries in MVC's are either moderate or major in severity. Clinically, it has been shown that intraparenchymal damage occurs in the

majority of patients who are admitted with blunt liver injury (67%) (John et al. 1992). Currently, no crash test dummies used to assess injury risk in MVC's are equipped to represent individual solid organs located asymmetrically in the human abdomen (Tamura et al. 2002). Thus, finite element models (FEMs) are being utilized to help reduce automotive related abdominal injuries. However, in order for the FEMs to provide accurate representation of human liver response to a blunt impact and correctly predict injury, they must be constructed with physical variables mechanically related to injury, such as stress and strain.

Multiple studies have been performed to address the mechanical response of whole livers to impact. Melvin et al. (1973) performed *in vivo* local impacts on livers of 17 Rhesus monkeys. Livers were excised from the monkey and placed on a load cell while still being perfused by the living animal. An electrohydraulic servo-controlled impactor was used to impact the livers. Ram displacement was varied to produce strains from 40-74%. Loading rate was varied from 5 cm/s to 500 cm/s. It was determined that the stress-strain behavior of the liver was affected by the loading rate, and onset of moderate trauma to the liver occurred at a stress level of 310 kPa. Injuries produced in the tests included subcapsular hemorrhaging and intraparenchymal damage. Wang et al. (1992) performed force-relaxation and creep experiments on diseased and nondiseased porcine livers using an indenter. They demonstrated that porcine liver tissue was a typical viscoelastic material and that normal and non-normal liver tissue had different biomechanical properties. Kerdok (2006) tested 4 porcine livers using a creep indention test. Each liver was impacted in-vivo, ex-vivo perfused, and ex-vivo nonperfused. The elastic and viscous responses were shown to be affected by perfusion. The biomechanical properties of the ex-vivo perfused liver were shown to be similar to that of the in-vivo perfused liver. However, the nonperfused livers were stiffer and more viscous and showed permanent strain deformation with repeated impacts. Sparks et al. (2007) impacted 14 fresh human livers with a rigid metal plate to a maximum deflection of 30% from the livers highest point. Peak applied stress varied between 157 kPa and 690 kPa with an average of 427 kPa to produce a 3+ MAIS injury. Impact energy and strain rate were highly correlated to injury, but the product of peak rate of tissue pressure increase and peak tissue pressure was shown to be the strongest correlate to injury. It is important to note that intraparenchymal damage was seen in 9 of the 14 livers tested and was consistent with injuries seen in CIREN cases. Impacts to intact livers have demonstrated the

viscoelastic characteristics of liver tissue, have shown that perfusion levels affect the material properties of liver tissue, and have revealed that the best indicator of injury is internal pressure in the parenchyma. However, these tests are limited by their ability to accurately calculate localized stress and strain. Therefore, in order to account for proper stress-strain relationships needed for FEMs, tissue level tension and compression tests need to be performed.

A few compression studies have been performed on isolated samples of liver parenchyma. A number of these studies have been limited to subfailure loading (Chui et al. 2004; Raghunathan et al. 2010; Roan and Vemaganti 2007; Tamura et al. 2002). However, two studies have performed failure tests. Seki and Iwamoto (1998) tested pieces of porcine heart (myocardium), liver, and spleen to determine a breaking stress. A specimen of tissue between 20-30 mm tall was placed in a cylindrical container (dia = 67 mm) with an open top and was compressed with an impactor (diameter = 5 mm). The container moved upward at 20 mm/min, corresponding to a strain rate of approximately 0.01 s^{-1}. It was determined that the breaking stress for the liver was 4.6 ± 0.3 kg/cm^2 (450.8 ± 29.4 kPa) with the capsule intact and 3.6 ± 0.3 kg/cm^2 (352.8 ± 29.4 kPa) without the capsule. The strain level at which the tissue broke was not described. Tamura et al. (2002) performed unconfined compression tests on porcine liver, spleen, and kidney samples at multiple loading rates. Each tissue specimen was preconditioned at 0.5 mm/sec for 5 cycles before a failure test was performed. The average ultimate compressive true stress for the liver was determined to be 123 kPa, 135 kPa, and 166 kPa for tests performed at 0.005 s^{-1}, 0.05 s^{-1}, and 0.5 s^{-1} respectively. The average ultimate compressive nominal strains for the liver were determined to be 0.432, 0.420, and 0.438 for tests performed at 0.005 s^{-1}, 0.05 s^{-1}, and 0.5 s^{-1} respectively. Because of the similarity in failure strains between rates, it was suggested that failure strain can be used as an injury criterion.

Although previous studies have provided insight into the mechanical response of liver parenchyma in unconfined compression, they are limited by their use of animal tissue and quasi-static strain rates. To accurately predict intraparenchyma damage to livers in MVCs, it is necessary to investigate the material response of human liver parenchyma in compressive loading. However, to the best of the author's knowledge there has been no attempt to quantify the viscoelastic response of human liver parenchyma in compressive loading. Thus, the purpose

of this study was to quantify the compressive material properties of human liver parenchyma at four distinct strain rates at static, quasistatic, and dynamic loading rates.

METHODS

A total of 36 unconfined compression tests were performed on the parenchyma of 6 unembalmed human livers obtained from Post Mortem Human Subjects (PMHS). Each liver was obtained within 36 hours of death and tested within 48 hours of death. NDRI (National Disease Research Interchange, Philadelphia, PA) supplied the livers. Subject sex, age, weight, and height, were tabulated along with the time to procurement from death and time to test completion from death (Table 12). All subjects were screened for medical issues that might affect the mechanical properties of the liver such as cancer in the abdomen or hepatitis. The livers were not frozen at any point during the transportation, preparation, and testing processes because it has been shown that freezing the tissue affects the biomechanical response (Santago et al. 2009b). All livers were immersed in Dulbecco's Modified Eagle's Medium (DMEM) prior to transportation, and transported with wet ice.

Table 12: Subject Information

Liver	Origin	Sex	Age	Weight	Height	Procurement Time	Testing completed
		(M/F)	(years)	(lbs)	(ft'in")	(hours post death)	(hours post death)
1	NDRI	M	55	N/A	N/A	14	48
2	NDRI	F	77	150	N/A	24	44
3	NDRI	F	70	N/A	N/A	24	48
4	NDRI	F	78	183	5'9"	15	40
5	NDRI	F	66	N/A	N/A	24	48
6	NDRI	F	73	150	5'5"	16	48

To test the parenchyma in unconfined compression, a cylindrically shaped compression sample was constructed. To create the samples, a uniform thickness slice of parenchyma first needed to be obtained. A custom blade assembly and slicing jig were utilized to create this slice (Figure 35). The blade assembly was constructed of multiple 48.3 cm long razor blades and spaced 10 mm apart by aluminum spacers. The slicing jig was constructed of aluminum U-shaped pieces spaced 5 mm apart to act as guides for the blades. A block of tissue was cut from the parenchyma of the liver and placed in the slicing jig (Figure 36). The block dimensions were determined such that the block would fit securely in the slicing jig. The blades on the blade assembly were aligned in the groves of the slicing jig. The slicing was performed with one smooth pass of the blades through the tissue block while minimizing downward force in order to avoid damaging or

deforming the tissue. Multiple specimens of constant thickness liver parenchyma were obtained after each slicing pass and.immersed in a DMEM bath.

Figure 35: Custom Slicing Jig (left) and Blade Assembly (right)

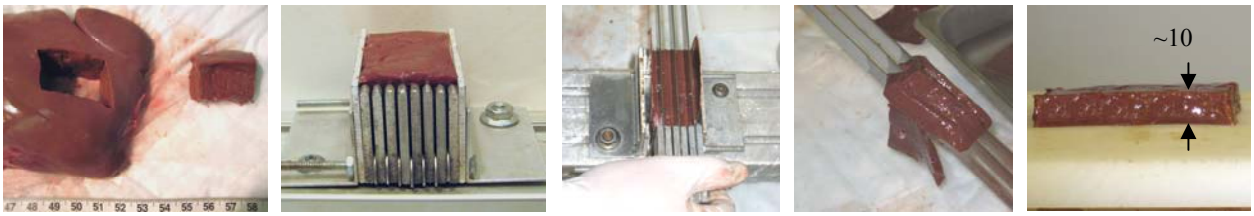

Figure 36: Slice Creation Methodology

To create a constant-diameter cylindrical tissue specimen, the edge of a 2.54 cm diameter steel tube was sharpened and used. The specimen was created by first placing the tissue slice on a cutting block. Sandpaper was placed on the cutting block to ensure the slice did not rotate while the sample was being prepared. A circular shaped hole was cut in the sandpaper to the keep the sandpaper from damaging the final tissue specimen. A cutting jig was placed on top of the tissue sample to hold the sample in place during cutting. The sharpened edge of the steel tube was aligned perpendicular to the tissue slice and rotated counterclockwise with minimal downward force to obtain the sample (Figure 37).

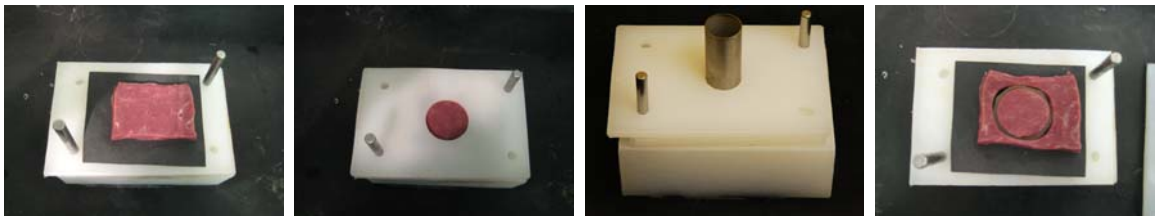

Figure 37: Specimen Creation Methodology

A custom testing setup was designed and utilized for the compression tests (Figure 38). A high rate servo-hydraulic Material Testing System (MTS 810, Eden Prairie, MN) was utilized to apply the compressive force to the tissue sample. A moveable plate was rigidly attached to base of the MTS. The plate was moveable so that impacting and reaction surfaces could be aligned. A load

cell (Interface 1210-AF-500lbf, Scottsdale, Arizona) was attached to plate, and the testing basin was attached to the top of the load cell. A load cell (Interface 1210-AF-500lbf, Scottsdale, Arizona) was screwed into the MTS piston, and the impacting surface was attached to the load cell. Both the reaction and impacting surfaces were constructed of polypropylene. An accelerometer (Endevco 7264B, 2000 g, San Juan Capistrano CA) was attached to impacting surface to measure the acceleration, which was utilized to inertially compensate the force. An aluminum beam was rigidly attached the MTS piston using a collet. A potentiometer (Space Age Control, 160-1705, 540mm, Palmdale, CA) was fastened to the moveable plate, and the string was attached to the aluminum beam to measure displacement of the impacting surface. Sampling rates used to acquire load cell data, accelerometer data, and potentiometer data are reported in Table 13.

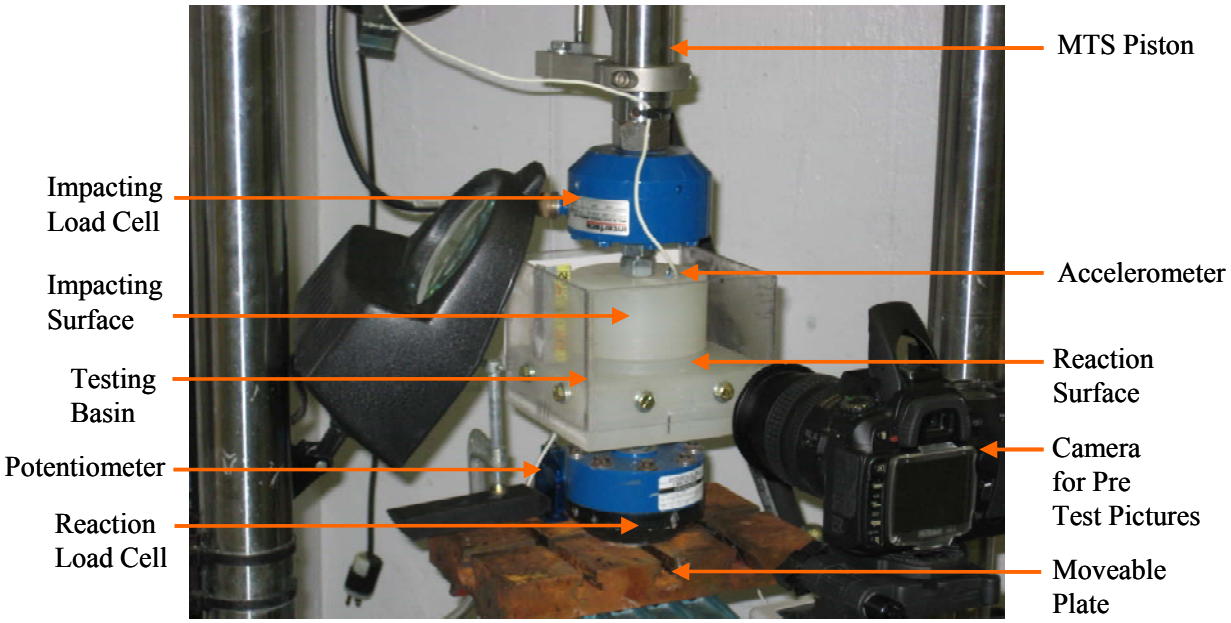

Figure 38: Testing Apparatus for Uniaxial Compression Tests

Table 13: Data Acquisition and Sampling Rates by Loading Rate

Rate	Desired Strain Rate (s^{-1})	Data Acquisition (kHz)
Rate 1	0.007	0.1
Rate 2	0.070	1.0
Rate 3	0.700	10.0
Rate 4	7.000	100.0

Before a series of tests was performed, verification was needed to ensure the surfaces were parallel. To achieve this, the MTS was lowered so that at maximum stroke there was a small gap between the impacting surface and the reaction surface. The impacting surface was raised slightly and a ball of hardening compound was placed at four distinct points around the edges of the surface interface. The impacting surface was then lowered into place, compressing the compound, which was then allowed to harden. After hardening, thickness measurements were taken at each location and compared to the other three. If all four thicknesses were within 0.13 mm of one another, the surfaces were considered parallel; otherwise, the bottom surface was shimmed and the process repeated. After determining that the surfaces were parallel, the initial gap height between the two surfaces needed to be determined. The impacting surface was raised, and hardening compound was placed at the center of the bottom surface. The impacting surface was then lowered, compressing the compound, which was allowed to harden. After hardening a thickness measurement was taken and this value was specified as the initial gap height (I) between the surfaces.

Before testing each tissue specimen, the specimen was heated in a DMEM bath for a minimum of 6 minutes. Prior to the specimen being removed from the bath, a Silicon Spray Lubricant was applied to each surface in the testing setup to ensure minimal friction between the specimen and each testing surface. Each specimen was removed from the bath and placed in the center of the reaction surface. Once the specimen was properly aligned in the testing setup, pretest pictures were taken from overhead and lateral positions, 985 pixels/in and 766pixels/in respectively, to determine initial specimen area and initial specimen height. The impacting surface was then moved into position 13mm above the maximum stroke. This gave the impactor surface time to accelerate to the desired velocity before reaching the sample. During the test, the impacting

surface moved toward the reaction surface at a constant velocity to produce one of the desired strain rates: 0.007 s^{-1}, 0.07 s^{-1}, 0.7 s^{-1}, or 7.0 s^{-1}.

Using an original Matlab code, force was plotted against time and a failure time was determined. The specimen was deemed to have failed when there was a significant drop in force (Figure 39). All data was then cut at the determined failure time. Force was then inertially compensated (F_{IC}) by multiplying the effective mass (m) by the acceleration (a) and subtracting this value from the raw force data (F) (eq. 11). Inertially compensated force was curve fit using an 11^{th} degree polynomial. Previous studies (Roan and Vemaganti 2007; Rosen et al. 2008) have utilized exponential curve fits for their data; however, exponential curve fits do not take into account the complexity of the load trace seen near the point of failure. Potentiometer data was also curve fit using a 5^{th} order polynomial (Manoogian et al. 2008). The average R^2 value for the force curve fit was 0.985±0.021 while the average R^2 value of the potentiometer curve fit was 0.998±0.001.

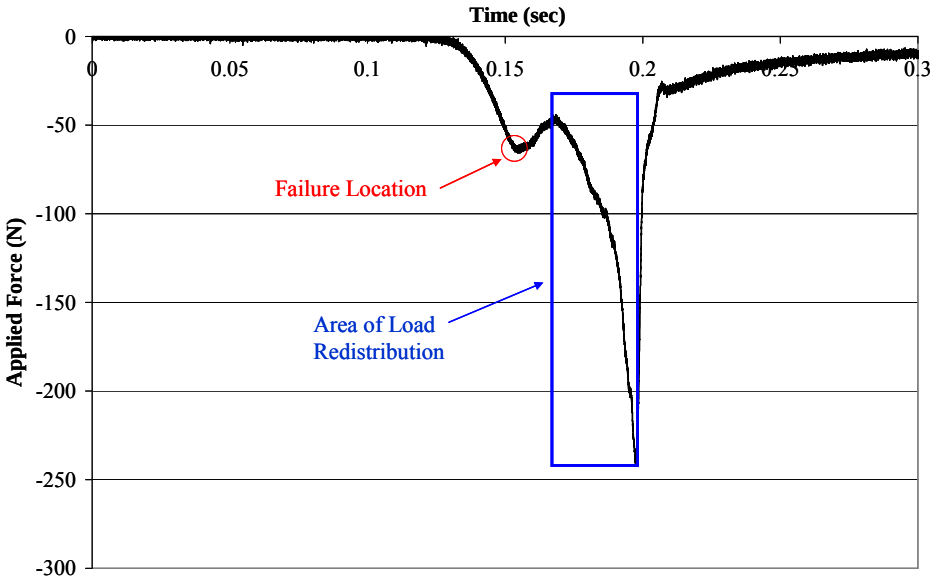

Figure 39: Typical Force versus Time Curve Showing Failure Location and Area of Load Redistribution

In order to calculate engineering stress, the initial area was determined from the pretest overhead pictures. For each overhead image, the tissue specimen was removed from the image by tracing the outline of the specimen and cropping the rest of the image. The subsequent image was input

into a custom Matlab code and a binary threshold was applied to the image so that the tissue sample was black and the rest of the image was white. Area was then determined by calculating the number of black pixels in the image and dividing by the number of pixels per inch in the image. Given the initial area cross sectional area (A_o) and curve fit force data (F_c) engineering stress (σ) was tabulated (eq. 12).

$$F_{IC} = F - m * a \quad \textbf{eq. 11}$$

$$\sigma = \frac{F_c}{A_o} \quad \textbf{eq. 12}$$

To calculate engineering strain, the tissue height was determined from the pretest lateral pictures. An average specimen height was determined by taking a measurement from both edges and the middle of the specimen. Once specimen height had been determined, an original Matlab code was utilized to determine strain. Specified pr test location of the impacting surface relative to the bottom of the stroke (S), typically 13mm, and the initial gap (I), described previously, were added to the curve fit potentiometer (P) data so that the location of the impactor surface relative to the reaction surface was known for the entire test ($Real_{Loc}$) (eq. 13). The final step in the process was to subtract the initial height of the tissue (L_o) from the output from eq. 13 so that the output (O) gave the location of the impacting surface relative to the initial height of the test specimen at each instance in time (eq. 14). At the time where the output from eq. 14 initially crosses or is equal to zero, the impacting surface is assumed to be in contact with the test specimen and that it would remain in contact for the remainder of the test. After time zero the output from eq. 14 corresponds to the change in height of the tissue sample (ΔL). Engineering strain (ε) can then be tabulated (eq. 15).

Characteristic engineering stress versus engineering strain curves were determined for all rates using a standard method (Lessley et al. 2004). An average failure stress and strain along with average strain rate was tabulated for each desired loading rate. A series of two-tailed Student's t-tests for means, assuming unequal variance, were performed to determine if there were significant differences in failure stress and failure strain due to the loading rate. Significance was defined as a two-tailed p-value of ≤ 0.05. Strain rate was determined by calculating the slope of the strain versus time curve between 25% and 75% of the maximum strain value.

$$\mathrm{Re}\, l_{Loc} = S + I + P \qquad \textbf{eq. 13}$$

$$O = \mathrm{Re}\, l_{Loc} - L_o \qquad \textbf{eq. 14}$$

$$\varepsilon = \frac{\Delta L}{L_o} \qquad \textbf{eq. 15}$$

RESULTS

A total of 36 unconfined failure compression tests were performed on human liver parenchyma at four different failure rates. All rates demonstrated a nonlinear stress versus strain response. For all specimens, failure was defined as a position of peak force before a significant drop in force (Figure 39). Engineering stress versus engineering strain curves for the uniaxial compression tests are shown. The data are reported as engineering stress and engineering strain. A total of 9 tests were performed at Rate 1 which had a desired strain rate of 0.007 s^{-1}. Stress versus strain data for Rate 1 is plotted with the corresponding characteristic average and standard deviations for failure stress and strain (Figure 40). Average failure stress and strain were -165.64 ± 41.76 kPa and -0.61 ± 0.05 respectively. Average strain rate was 0.008 ± 0.001 s^{-1}. A total of 9 tests were performed at Rate 2, which had a desired strain rate of 0.07 s^{-1}. For Rate 2 each test stress versus strain data is plotted with the corresponding characteristic average and standard deviations for failure stress and strain (Figure 41). Average failure stress and strain were -158.42 ± 43.10 kPa and -0.52 ± 0.04 respectively. verage strain rate was 0.074 ± 0.001 s^{-1}. A total of 9 tests were performed at Rate 3, which had a desired strain rate of 0.7 s^{-1}. Stress versus strain data for Rate 3 is plotted with the corresponding characteristic average and standard deviations for failure stress and strain (Figure 42). Average failure stress and strain were -192.60 ± 52.62 kPa and -0.46 ± 0.05 respectively. Average strain rate was 0.776 ± 0.104 s^{-1}. A total of 9 tests were performed at Rate 4, which had a desired strain rate of 7.0 s^{-1}. For Rate 4 each tests stress versus strain data is plotted with the corresponding characteristic average and standard deviations for failure stress and strain (Figure 43). The average failure stress and strain were -203.02 ± 33.75 kPa and -0.46 ± 0.05, respectively. Average strain rate was 8.011 ± 0.834 s^{-1}. The characteristic average stress versus strain curve for each rate was plotted so that a clear comparisons could be

made (Figure 44). P-values for all comparisons have been tabulated (Table 14). Bold values indicate significance.

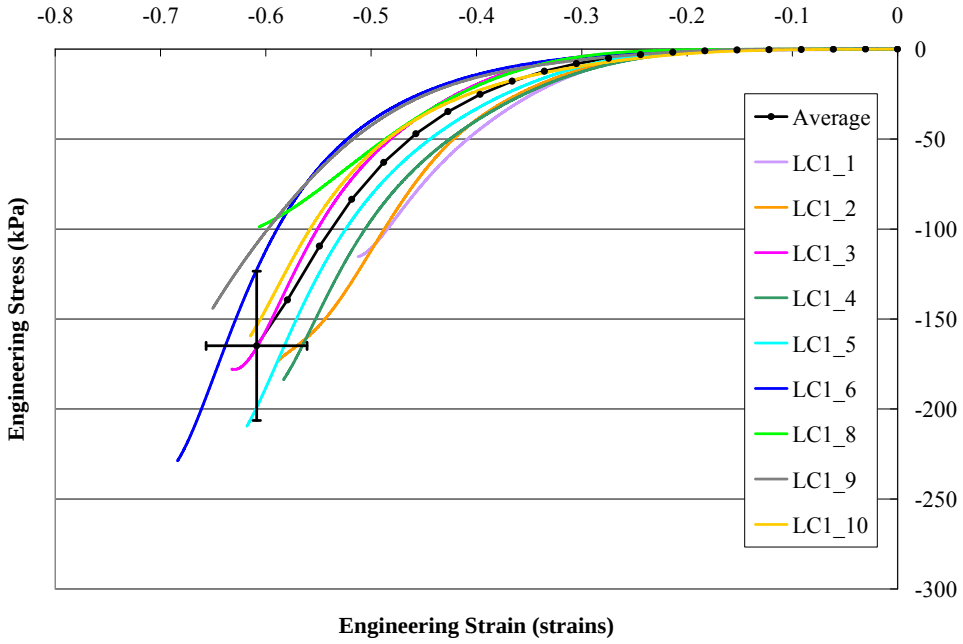

Figure 40: Stress vs. Strain data for the tests conducted at 0.008 s-1 and associated characteristic average

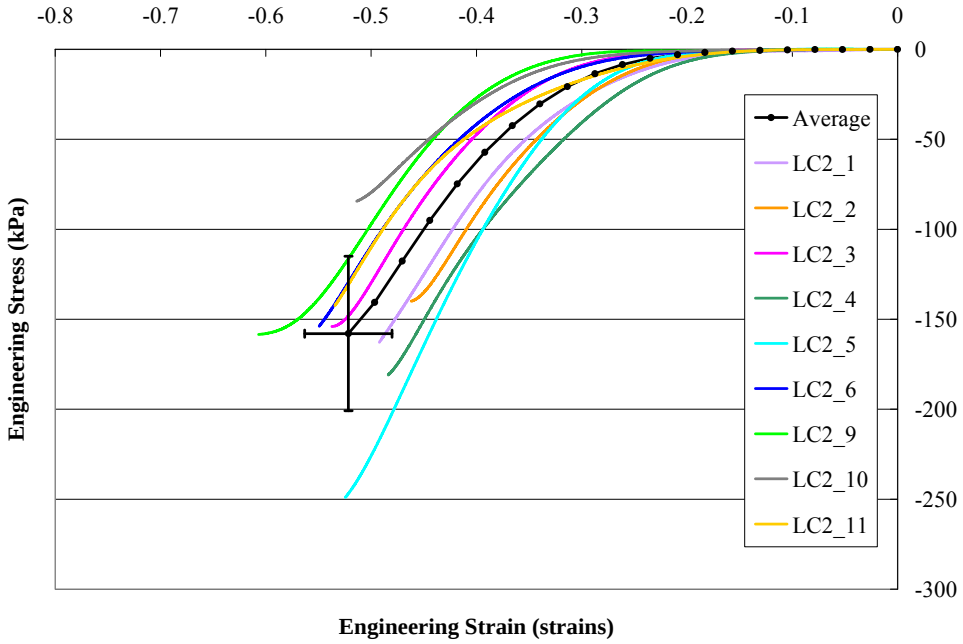

Figure 41: Stress vs. Strain data for the tests conducted at 0.074 s-1 and associated characteristic average

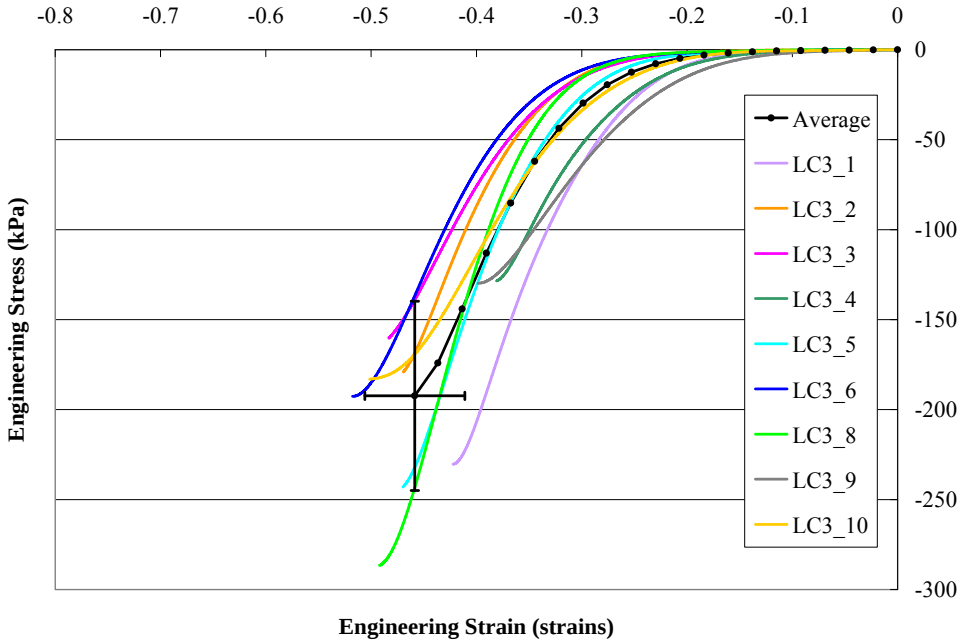

Figure 42: Stress vs. Strain data for the tests conducted at 0.776 s-1 and associated characteristic average

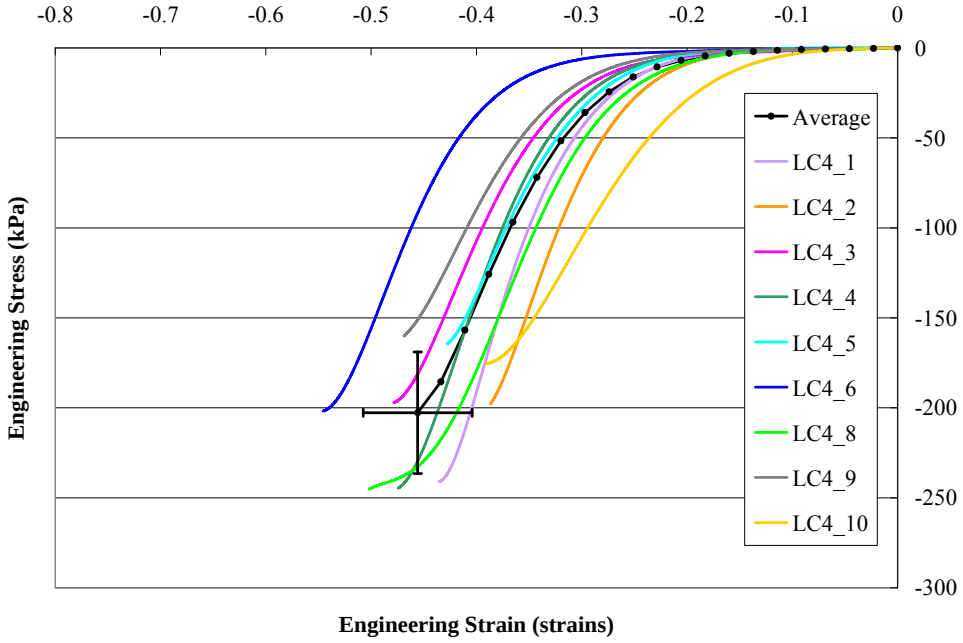

Figure 43: Stress vs. Strain data for the tests conducted at 8.011 s-1 and associated characteristic average

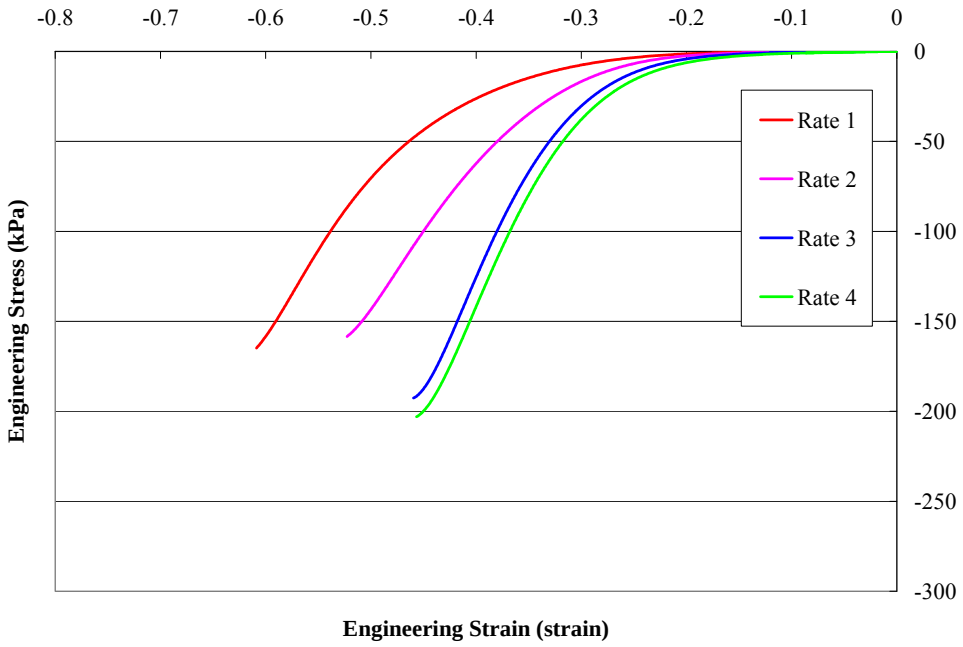

Figure 44: Characteristic Averages for Each Rate

Table 14: Two-tailed Student-t-test p-values for comparisons made in between each loading rate.

Comparison	Strain	Stress
	p-value	p-value
Rate 1 to Rate 2	< **0.01**	0.72
Rate 1 to Rate 3	< **0.01**	0.25
Rate 1 to Rate 4	< **0.01**	**0.05**
Rate 2 to Rate 3	< **0.01**	0.15
Rate 2 to Rate 4	< **0.01**	**0.03**
Rate 3 to Rate 4	0.91	0.63

DISCUSSION

This study is the first to present stress versus strain data and failure information for human liver parenchyma tested in unconfined compression. Most of the variance seen in the data can be attributed to specimen variability because all of the specimens were prepared and tested in an identical way. Although the parenchyma has some irregularities, special care was taken to avoid

these during the cutting process. However, the existence of small non-visible vasculature inside the tissue samples is unavoidable would contribute to the specimen variation.

It was determined, from these tests that the human liver has a non-linear stress versus strain response and some statically significant rate dependence. Average failure strain showed significance between all rates except between Rates 3 and 4. However average failure stress only showed significance between Rate 1 and Rate 4 and Rate 2 and Rate 4.

Although there have been no previous studies testing human liver parenchyma in unconfined compression, failure properties of porcine liver parenchyma developed from unconfined compression have been reported (Tamura et al. 2002). Before a direct comparison between the porcine data from Tamura et al (2002) and the current study could be made, the data from the current study needed to be converted to true stress and nominal strain. Tamura et al. (2002) assumed constant volume for the tissue samples so instantaneous area was determined by dividing the pre test volume by the instantaneous height. Tamura et al (2002) also utilized an arbitrary load of 0.6 N to correspond with the zero strain location. Data from the current study was shifted to correspond with this. Data from the current study collected from Rate 1, Rate 2, and Rate 3 were considered comparable to the 0.005 s^{-1}, 0.05 s^{-1}, and 0.5 s^{-1} strain rates utilized for the porcine data (Figure 45). Failure stress reported by Tamura et al. (2002) was shown to be significantly higher for all rates compared to the current study. This discrepancy can be explained by the difference in cellular structure between porcine and human liver. The lobule is the functional unit of the liver (Guyton and Hall 2006). The lobule has a cylindrical shape with central vein passing through its core surrounded by radiating sheets of hepatocyte cells (Saladin and McFarland 2008). It has been previously demonstrated that human liver parenchyma has a similar lobule to that of porcine liver parenchyma; however, the thin septa of collagenous supporting tissue seen in the porcine liver parenchyma is absent in the human liver parenchyma (Burkitt et al. 1993). It has also been previously demonstrated that as the percentage of connective tissue content increases that stiffness increases (Mazza et al. 2007). Because the porcine liver has a larger amount of connective tissue than the human liver, failure stress for the porcine liver parenchyma would be higher.

Tamura et al. (2002) also showed constant failure strain for all rates (Figure 46). Unlike the current study, each porcine sample was preconditioned before each failure test and the samples were frozen prior to specimen preparation. Kerdok et al. (2006) found that repeated indentions to an unperfused liver resulted in permanent strain deformation. The samples Tamura et al (2002) tested were not perfused; therefore, the preconditioning would cause a similar reaction to what was described by Kerdok et al (2006) for the repeated indentions. Permanent strain deformation could rid the sample of a toe region, or the region where there is strain increase with minimal stress increase. This might cause the consistent failure strain between each rate that was shown by Tamura et al. (2002).

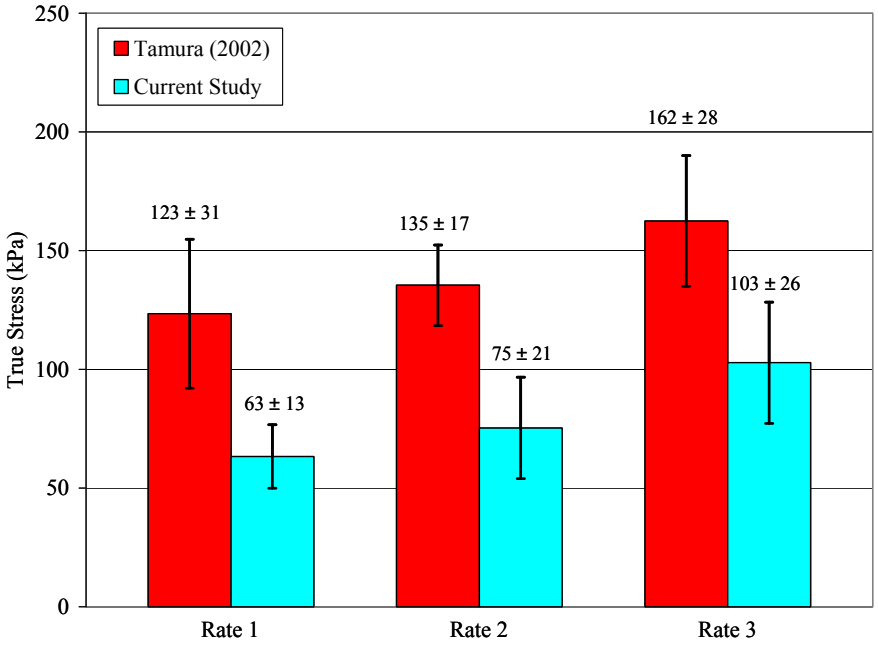

Figure 45: Failure Stress Comparison between Tamura (2002) and Current Study

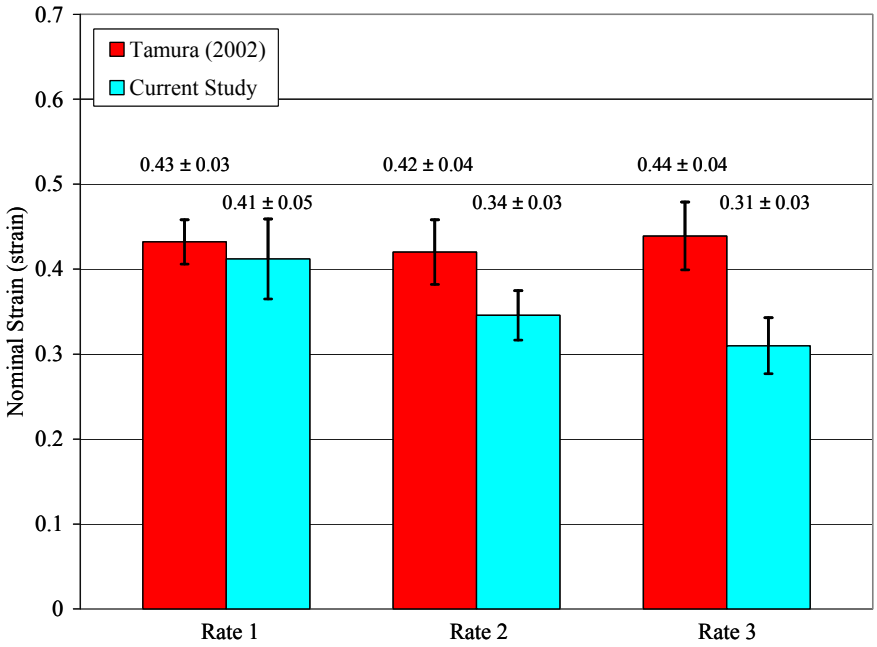

Figure 46: Failure Strain Comparison between Tamura (2002) and Current Study

The comparison of the current study to a previous study involving animal tissue (Tamura et al. 2002) illustrates that differences in cellular structure between animal and human liver can result in significant differences in the material response. Although material testing performed on animal tissue provides valuable insight into the material response of liver, this study demonstrates that it is imperative to perform material testing on human tissue in order to determine accurate tissue level tolerance values for FEMs used to predict injuries in vehicle occupants.

It is important to note that it is difficult to define the exact point at which tissue failure occurs in compressive loading. Failure in compressive loading is generally defined as the peak load or inflection point. However, tissue failure could occur prior to this point. To explain, in compressive loading the load can either continually increase after the tissue begins to fail, or begin to increase again once the tissue has failed and the load has dropped because with continued compression passed failure the load is redistributed throughout the sample (Figure 39).

The current study made every attempt to create a nearly frictionless interface between the impacting surfaces and the tissue specimen. The lack of barreling seen in the tests was a good

indication of a nearly frictionless interface (Figure 47). It has been previously demonstrated, however, that for soft biological tissue even a small friction coefficient (0.01) can have a substantial impact on the reaction force (7%) (Miller 2005). However, a no-slip condition can not be utilized for the current study because of high strains seen in the current study (Miller 2005). At high strains the assumption that planes perpendicular to the direction of force remain plane does not hold true for a no-slip interface (Miller 2005). A method for obtaining the friction coefficient has been previous proposed and should be utilized in the future to obtain a true coefficient of friction (Wu et al. 2004).

Figure 47: Still Frames of a Typical Unconfined Compression Tests

There are limitations with this study. A total of 27% of the resting cardiac output flows through the liver each min (Guyton and Hall 2006). In order to take this into consideration, the samples were kept saturated with DMEM prior to testing. However, blood flow and pressure *in vivo* was not taken into consideration. Warm ischemia time for each subject is also unknown and has been shown to negatively affect initial graft function during transplants (Platz et al. 1997). Post mortem procurement time and post mortem test completion time vary widely. These factors could contribute to tissue degradation, thereby affecting the biomechanical properties of the liver tissue.

CONCLUSIONS

This study presents a total of 36 unconfined compression tests on human liver v. A total of 6 livers were utilized to acquire cylindrical shaped compression specimens for testing at four distinct loading rates: 0.008 s^{-1}, 0.074 s^{-1}, 0.776 s^{-1}, and 8.011 s^{-1}. Average failure stresses of -165.64 ± 41.76 kPa, -158.42 ± 43.10 kPa, -192.60 ± 52.62 kPa, and -203.02 ± 33.75 kPa were seen for each loading rate respectively. Average failure strains of -0.61 ± 0.05, -0.52 ± 0.04, -0.46 ± 0.05, and -0.46 ± 0.05 were seen for each loading rate respectively. Rate dependence was

seen with failure stress increasing with increasing strain rate and failure strain decreasing with increasing strain rate. Statically significant rate dependence was seen between all rates except between Rate 3 and Rate 4 for average failure strain. However, statistical significance was only seen between Rate 1 and Rate 4 and between Rate 2 and Rate 4 for average failure stress. When compared to previous unconfined compression tests, the current study addresses the material response to strictly the human liver parenchyma as well as addresses the need for dynamic loading rates. In summary, failure compressive material properties for the parenchyma of the human liver have been discovered at static, quasistatic, and dynamic loading rates for use as material properties and injury tolerance values to validate finite element models.

ACKNOWLEDGEMENTS

The author would like to acknowledge the Toyota Motor Corporation for their funding and support.

REFERENCES

Augenstein JS, Bowen J, Perdeck EB, Singer M, Stratton JE, Horton T, Rao A, Digges KH, Malliaris AC, Steps J. 2000. Injury patterns in near-side collisions. SAE 2000 World Congress: SAE International.

Bondy N. 1980. Abdominal Injuries in the National Crash Severity Study. National Center for Statistics and Analysis. 59-80 p.

Burkitt HG, Young B, Heath JW. 1993. Liver and pancreas. Wheater's Functional Histology: A Text and Colour Atlas. 3rd ed. New York: Churchhill Livingstong. p 272-277.

Christmas AB, Wilson AK, Manning B, Franklin GA, Miller FB, Richardson JD, Rodriquez JL. 2005. Selective managment of blunt hepatic injuries including nonoperative management is a safe and effective strategy. Surgery 138(4):606-610.

Chui C, Kobayashi E, Chen X, Hisada T, Sakuma I. 2004. Combined compression and elongation experiments and non-linear modelling of liver tissue for surgical simulation. Medical and Biological Engineering and Computing 42(5):787-798.

Dyce KM, Sack WO, Wensing CJG. 2002a. The Abdomen of the Pig. Textbook of Veterinary Anatomy. 3rd ed. Philadelphia: Saunders. p 781-782.

Dyce KM, Sack WO, Wensing CJG. 2002b. The Abdomen of the Ruminants. Textbook of Veterinary Anatomy. 3rd ed. Philadelphia: Saunders. p 685-686.

Elhagediab AM, Rouhana SW. Patterns of Abdominal Injury in Frontal Automotive Crashes; 1998; Windsor, Ontario, Canada.

Guyton AC, Hall JE. 2006. Textbook of Medical Physiology. New Delhi, India: Elsevier. 1116 p.

Holbrook TL, Hoyt DB, Eastmen AB, Sise MJ, Kennedy F, Velky T, Conroy C, Pacyna S, Erwin S. 2007. The Impact of Safety Belt Use on Liver Injuries in Motor Vehicle Crashes: The Importance of Motor Vehicle Safety Systems. Journal of Trauma 63(2):300-306.

Hollenstein M, Nava A, Valtorta D, Snedeker JG, Mazza E. 2006. Mechanical Characterization of the Liver Capsule and Parenchyma. In: Szekely MHG, editor. Biomedical Simulation. Berlin/Heidelberg: Springer-Verlag. p 150-158.

Hurtuk M, Reed RLI, Esposito TJ, Davis KA, Luchette FA. 2006. Trauma surgeons practice what the preach: The NTDB story on solid organ injury management. Journal of Trauma 61(2):243-255.

John TG, Greig JD, Johnstone AJ, Garden OJ. 1992. Liver Trauma: A 10-year experience. British Journal of Surgery 79(12):1352-1356.

Kerdok AE, Ottensmeyer MP, Howe RD. 2006. Effects of perfusion on the viscoelastic characteristics of liver. Journal of Biomechanics(39):2221-2231.
Lessley D, Crandall J, Shaw G, Funk J, Kent R. 2004. A Normalization Technique for Developing Corridors from Individual Subject Responses. SAE Technial Paper Series. Detriot, MI.
Manoogian SJ, Bisplinghoff JA, McNally C, Kemper AR, Santago AC, Duma SM. 2008. Dynamic tensile properties of human placenta. Journal of Biomechanics 41(16):3436-3440.
Mazza E, Nava A, Hahnloser D, Jochum W, Bajka M. 2007. The mechanical response of human liver and its relation to histology: An in vivo study. Medical Image analysis 11(6):663-672.
Melvin JW, Stalnaker RL, Roberts VL, Trollope ML. Impact Injury Mechanisms in Abdominal Organs; 1973; Oklahoma City, OK. SAE. p 115-126.
Miller K. 2005. Method of testing very soft biological tissues in compression. Journal of Biomechanics 38(1):153-158.
Platz KP, Mueller AR, Schafer C, Jahns S, Guckelberger O, Neuhaus P. 1997. Influence of Warm Ischemia Time on Initial Graft Function in Human Live Transport. Transplantation Proceedings 29(8):3458-3459.
Raghunathan S, Evans D, Sparks JL. 2010. Poroviscoelastic Modeling of Liver Biomechanical Response in Unfonfined Compression. Annals of Biomedical Engineering.
Roan E, Vemaganti K. 2007. The Nonlinear Material Properties of Liver Tissue Determined from N0-Slip Uniaxial Compression Experiments. Journal of Biomedical Engineering 129:450-456.
Rosen J, Brown JD, De S, Sinanan M, Hannaford B. 2008. Biomechanical Properties of Abdominal Organs In Vivo and Postmortem Under Compression Loads. Journal of Biomechanical Engineering 130(2):021020.
Saladin KS, McFarland RK. 2008. Human Anatomy 2nd Edition. 771 p.
Santago AC, Kemper AR, McNally C, Sparks JL, Duma SM. 2009a. The effect of temperature on the mechanical properties of bovine liver - biomed 2009. Biomed Sci Instrum 45:376-81.
Santago AC, Kemper AR, McNally C, Sparks JL, Duma SM. 2009b. Freezing affects the mechanical properties of bovine liver - biomed 2009. Biomed Sci Instrum 45:24-9.
Seki S, Iwamoto H. 1998. Disruptive Forces for Swine Heart, Liver, and Spleen: Their Breaking Stresses. Journal of Trauma: Injury, Infection, and Critical Care 45(6):1079-1083.
Sparks JL, Bolte IV JH, Dupaix RB, Jones KH, Steinberg SM, Herriott R, Stammen J, Donnelly B. 2007. Using Pressure to Predict Liver Injury Risk from Blunt Impact. Stapp Car Crash J. p 401-432.
Stingl J, Baca V, Cech P, Kovanda J, Kovandova H, Mandys V, Rejmontova J, Sosna B. 2002. Morphology and some biomechanical properties of human liver and spleen. Surgical and Radiological Anatomy 24(5):285-289.
Tamura A, Omori K, Miki K, Lee JB, Yang KH, King AI. 2002. Mechanical characterization of porcine abdominal organs. Stapp Car Crash J 46:55-69.
Thor CP. 2008. Characteristics of Thoracic Organ Injuries in Frontal Crashes. Blacksburg: Virginia Polytechnic Institute and State University.
Uehara H. 1995. A study on the mechanical properties of the kidney, liver, and spleen, by means of tensile stress test with variable strain velocity. Journal of Kyoto Prefectural University of Medicine 104(1):439-451.
Van Ee CA, Chasse AL, Myers BS. The Effect of Postmortem Time and Freezer Storage on the Mechanical Properties of Skeletal Muscle; 1998; Tempe, Arizona. Society of Automotive Engineers.
Wang BC, Wang GR, Yan DH, Liu YP. 1992. An Experimental Study on Biomechanical Properties of Hepatic Tissue Using a New Measuring Method. Bio-Medical Materials and Engineering 2:133-138.
Wu JZ, Dong RG, Smutz WP. 2004. Elimination of the friction effects in unconfined compression tests of biomaterials of soft tissues. Proceedings of the Institution of Mechanical Engineering. Part H Journal of Engineering in Medicine 218(1):35-40.
Yamada H. 1970. Strength of Biological Materials. Baltimore: The Williams and Wilkins Company.